Computers and Electronics in Agriculture 193 (2022) 106687

Contents lists available at ScienceDirect

Computers and Electronics in Agriculture

journal homepage: www.elsevier.com/locate/compag

Combined Terrestrial Evapotranspiration Index prediction using a hybrid artificial intelligence paradigm integrated with relief algorithm-based feature selection

Mehdi Jamei [a,*], Ahmed Elbeltagi [b,c], Saman Maroufpoor [d], Masoud Karbasi [e], Mozhdeh Jamei [f,g], Mohammadnabi Jalali [h], Negin Najafzadeh [i]

[a] Faculty of Engineering, Shohadaye Hoveizeh Campus of Technology, Shahid Chamran University of Ahvaz, Dashte Azadegan, Iran
[b] Agricultural Engineering Department, Faculty of Agriculture, Mansoura University, Mansoura 35516, Egypt
[c] College of Environmental and Resource Sciences, Zhejiang University, Hangzhou 310058, China
[d] Department of Irrigation and Reclamation Engineering, University of Tehran, Tehran, Iran
[e] Faculty of Agriculture, University of Zanjan, Zanjan, Iran
[f] Water Science and Engineering Department, Ferdowsi University of Mashhad, Mashhad, Iran
[g] Khuzestan Water and Power Authority, Ahvaz, Iran
[h] Department of Water Engineering, Aburaihan Campus, University of Tehran, Iran
[i] Department of Water Engineering, Faculty of Agriculture, University of Tabriz, Tabriz, Iran

ARTICLE INFO

Keywords:
Terrestrial Evapotranspiration Index
Drought
Whale optimization algorithm
Relief algorithm
ANN
LSSVR

ABSTRACT

Drought is a common environmental disaster strongly influenced by the potential production of agricultural products, lack of water resources, and yields destructive effects on the economy. In this study, the prediction of a novel monthly Combined Terrestrial Evapotranspiration Index (CTEI) was considered as a measure of all three types of drought (meteorology, hydrology, and agriculture) in the Ganga river basin (GRB) over the period of 14 years. For this purpose, a combination of hydro-meteorological and satellite-based data, including 11 input variables, was implemented. A new Artificial Neural Network (ANN) integrated with a Whale Optimization Algorithm (WOA-ANN) and a Relief algorithm-based Feature Selection (FS) method was applied to simulate the monthly CTEI index and find the optimum input combinations. Besides, the standalone ANN and Least Square Support Vector Regression (LSSVR) models were examined to validate the WOA-ANN performance. The results indicated that WOA-ANN with (R = 0.9391), (RMSE = 0.241), (WI = 0.968), and ($U_{95\%}$ = 0.669) had a high ability to predict CTEI and reduced the RMSE in the ANN and LSSVR models by 27% and 30%, respectively. WOA-ANN had the best predictive performance, followed by LSSVR and ANN models, respectively, concerning various graphical validations and diagnostic analyses. Besides, the outcome of this research, despite fewer parameters (seven parameters), considerably outperformed the study of (Elbeltagi et al., 2021) with (R = 0.9055 and RMSE = 0.33) accuracy employing 11 inputs.

1. Introduction

Drought is one of the quiet and creeping climatic natural disasters, which can have devastating and harmful effects in various economic, social, and environmental fields (Botai et al., 2016; Li et al., 2020). The effects of drought will remain in the region for many years if appropriate solutions are not implemented (Ashok K Mishra and Singh, 2011). Drought is a phenomenon that occurs slowly, causes significant water resource changes, and affects different resources and sectors, including agriculture and natural resources(Wilhite and Glantz, 1985). The occurrence of severe droughts in Africa, India, North America, China, Australia, and the Middle East in recent decades indicates the vulnerability of developed and developing societies to drought (De Kauwe et al., 2020, Miyan, 2015, Zhao et al., 2020, Ahmadalipour et al., 2019; Ide, 2018). Due to the increasing population and demand for water resources and their role in development, vulnerability to drought in communities

* Corresponding author.
E-mail addresses: M.Jamei@shhut.ac.ir (M. Jamei), S.maroufpoor@ut.ac.ir (S. Maroufpoor), m.karbasi@znu.ac.ir (M. Karbasi), mozhdeh.jamei@gmail.com (M. Jamei), Mn.jalali99@ut.ac.ir (M. Jalali), Negin.najafzadeh99@gmail.com (N. Najafzadeh).

https://doi.org/10.1016/j.compag.2022.106687
Received 3 August 2021; Received in revised form 1 January 2022; Accepted 3 January 2022

increases (Zhang et al., 2017; Elbeltagi et al., 2020). Therefore, quantitative analysis of drought needs a suitable indicator to accurately determine wet and dry periods (Zhang et al., 2017). Several indicators for drought monitoring can be classified into two general categories: univariate and multivariate(Liu et al., 2019; Zengir et al., 2020). Researchers have developed more than 150 different indicators to monitor and evaluate different types of drought (agricultural, hydrological and, meteorological) (Li et al., 2020). Meanwhile, some of these indices such as standardized precipitation index (SPI) (McKee et al., 1993), Palmer drought severity index(PDSI) (Alley, 1984), reconnaissance drought index (RDI) (Tsakiris and Vangelis, 2005), and standardized precipitation evapotranspiration index (SPEI) (Vicente-Serrano et al., 2010) have become more common and have been considered.

Dharpure et al. (2020) developed a novel drought index, namely, CTEI, which in addition to the difference in potential evapotranspiration (PET) and precipitation (P), also considers the surface and subsurface water column (GRACE data). The advantages of the CTEI drought index over other indices include 1) Simplicity of calculation, 2) Consideration of potential evapotranspiration, an indicator of global warming, and the growing demand for fresh water and its stress on groundwater. 3) GRACE observations are beneficial in presenting water column storage changes on a monthly scale. Therefore, the CTEI index can be more accurate in estimating drought events by considering the water storage component, which is regarded as in the current research for AI-based modeling.

Developing a model that can forecast drought is an essential step in reducing the destructive effects of drought. In arid and semi-arid areas, providing accurate time information on drought risk can be the basis for long-term water resources management and related decisions (Mulualem and Liou, 2020). In recent years, many types of research have been conducted to forecast droughts in different parts of the world (Morid et al., 2007, Y. Zhang et al., 2019, Trambauer et al., 2013; Madadgar and Moradkhani, 2014) so that through this research and have enough information about this natural phenomenon, effective and efficient steps can be taken to manage it properly. Recently the application of various Machine Learning (ML) technics to forecast different climatic time series has become very popular (Cifuentes et al., 2020; Maroufpoor, 2019; Papacharalampous et al., 2018; Yaseen et al., 2018). Drought forecasting has also been considered due to its high relationship with climatic time series. Among the ML methods used in drought, prediction is ANN (A K Mishra et al., 2007, Cutore et al., 2009; Kousari et al., 2017), support vector regression (SVR)(Deng et al., 2011; Deo et al., 2017), extreme learning machine (Ali et al., 2018; Deo and Şahin, 2015), fuzzy logic(Keskin et al., 2009; Özger et al., 2012), adaptive neuro-fuzzy inference system (ANFIS) (Bacanli et al., 2009, Mokhtarzad et al., 2017; Nguyen et al., 2017) and ensemble (Li et al., 2020; Fundel et al., 2013) models.

Deo and Şahin (2015) forecasted the SPEI index at selected meteorological stations in Australia using an ANN. A neural network with an architecture of 18-43-1 (input, hidden, and output neurons) was recognized as the top architecture. The results RMSE and R^2statistics showed that the ANN model could forecast drought. Similar results have been reported by Ali et al. (2017) in forecasting drought in northern Pakistan. Kisi et al. (2019) used ANFIS combined with four metaheuristic algorithms, including PSO (Particle Swarm Optimization), BOA (Butterfly Optimization Algorithm), ACO (Ant Colony Algorithm), and GA (Genetic Algorithm), to forecast SPI drought index in several stations in a semi-arid region of Iran. Their results showed that the ANFIS-PSO model had the highest accuracy in most stations. Zhang et al. (2019) used two methods, the cross-correlation function and the distributed lag normal method (DLNM), to select the optimal inputs (predictors) of the ANN and XGBoost models to forecast the SPEI index for the next 1 to 6 months at 32 Chinese meteorological stations. The results show the superiority of the DLNM method in determining the optimal inputs and XGBoost in drought forecasting. In another study, Mulualem and Liou (2020) Mohamed and Karem, 2018 used an ANN-based model to predict the SPEI drought index in the upstream Blue Nile. Their results reveal the high capability of the ANN model in predicting drought. Moreover, Özger et al. (2020) used three ML models (SVR, ANFIS, and M5) combined with two-time series preprocessing technics [Wavelet Decomposition (WD) and Empirical Mode Decomposition (EMD)] to forecast self -calibrated PDSI (SC-PDSI). They reported significant improvement of ML model's performance by the introduction of WD and EMD technics. Khan et al. (2020) predicted the SPEI index in Pakistan using the NCEP / NCAR database and SVR, ANN, and KNN (K nearest neighbor) ML models. They also used a method called RFE (Recursive Feature Elimination) to determine the optimal inputs. The authors' results showed that the SVR model has a higher ability to identify drought's temporal and spatial characteristics. A review of the literature has shown an attempt to predict drought with different indicators. While each of these indicators monitors a specific type of drought. Recently, researchers several efforts have been devoted to drought indices using machine learning methods (Beyaztas and Yaseen, 2019; Malik et al., 2020, 2021d, 2021a; Malik and Kumar, 2020; Yaseen et al., 2021; Yaseen and Shahid, 2020). For instance, (Malik et al., 2020) studied on multiple scales of SPI at six meteorological sites using co-active neuro-fuzzy inference system (CANFIS), multiple linear regression (MLR), and MLP models. Besides, Malik et al.(Malik et al., 2021c) developed a predictive model based on SVR integrated with Particle Swarm Optimization (PSO) and Harris Hawks Optimization (HHO) algorithm to forecast one month ahead of effective drought index (EDI) at various sites of Uttarakhand State of India. More recently, Karbasi et al. provided a complementary model including three ML models (Gaussian Process Regression (GPR), Cascaded Forward Neural Network (CFNN), and ANN) integrated wavelet decomposition transform (DWT) to forecast the multi-scalar SPEI drought index for one to six months ahead (Karbasi et al., 2021b).

In the present study, the monthly CTEI index was considered an indicator representing all types of drought (meteorological, hydrological, and agricultural). The CTEI has a high ability to describe drought in areas due to the consideration of precipitation (P), surface and groundwater storage, soil moisture, and other hydrological parameters in its procedure. The main objective of this study is to predict the monthly CTEI index based on the WOA-ANN along with Relief algorithm-based feature selection (FS) over 14 years in the Ganga river basin. The ability of the WOA-ANN was evaluated against standalone ANN and LSSVR models using various training algorithms and kernel functions, respectively. To the best of the authors' knowledge, monthly CTEI prediction using hybrid ML models optimized with a FS scheme has not been made before.

2. Material and methods

2.1. Study area

The Ganga river basin (GRB) is one of the most populous (about 440 million people) river systems in the World (Anand et al., 2018). The basin is situated in the northern part of the country and lies between latitude 21°32′8.6″ - 31°27′36.2″ N and longitude 73°14′33.4″ - 90°53′18.9″ E, over an area of 10,86,000 km^2 (Fig. 1). The GRB outspreads in four countries, i.e., India (79%), Nepal (14%), Bangladesh (4%), and China (3%). In India, it covers 8,61,452 km^2, nearly 26% of its total geographic area (India-WRIS, 2012). The GRB originates in the Himalayan Mountains at the snout of the Gangotri glacier at an elevation of ~7000 m a.s.l. The confluence of the Bhagirathi River and Alaknanda Rivers joins in the town of Devprayag, then officially called the Ganga River. The main tributaries of the Ganga River are the Yamuna, the Ramganga, the Gomti, the Ghaghra, the Sone, the Gandak, the Kosi, and the Mahananda. And, it flows for about 2,510 km, generally southeastward, through a vast plain to the Bay of Bengal.

The primary source of water in the Ganga River is a surface runoff generated by precipitation (~66%), base flow (~14%), glacier melt

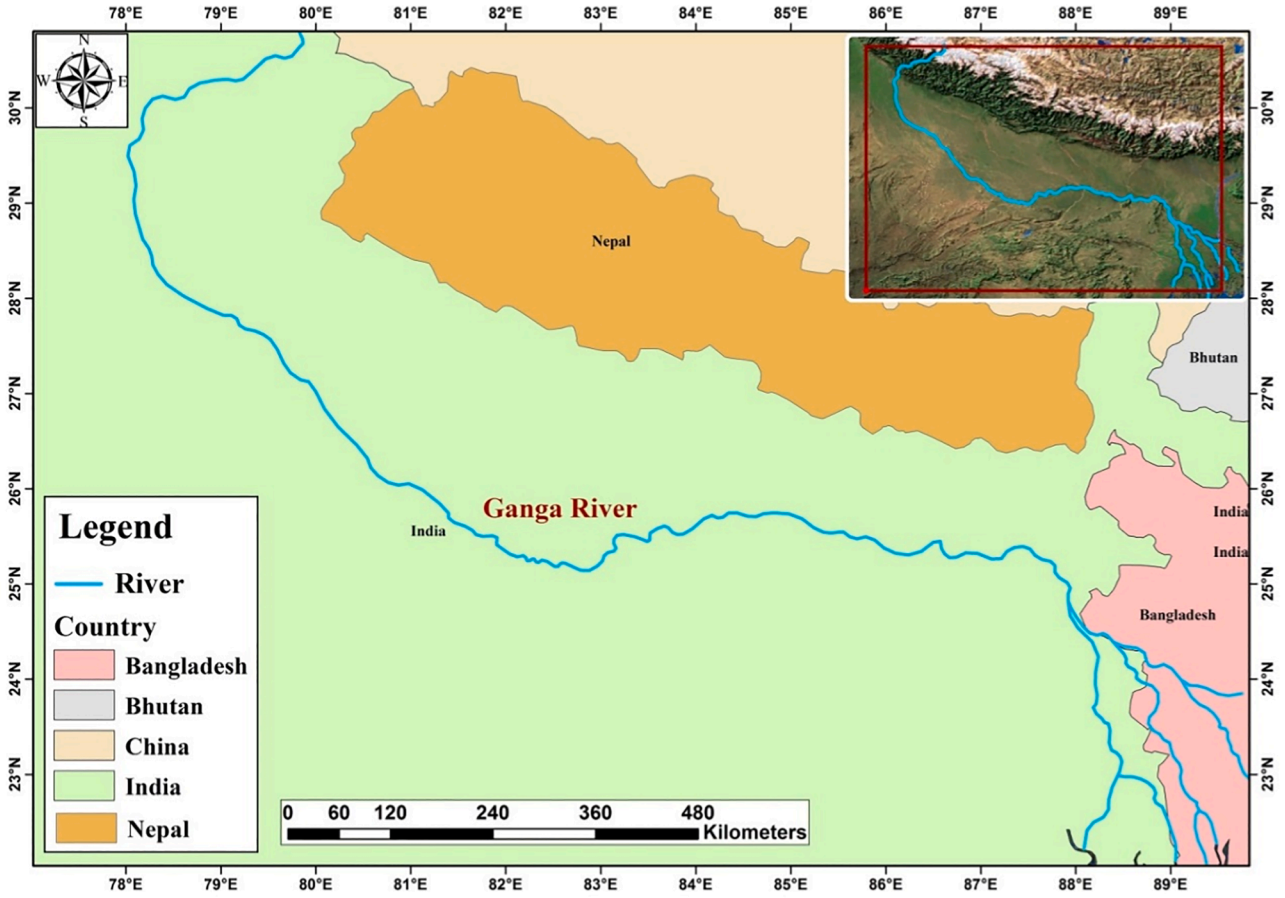

Fig. 1. Location map of the Ganga river basin and its tributaries.

(~11.5%), and snowmelt (~8.5%). The GRB received 84% of total rainfall during the monsoon season (June to October). The monsoon season accounts for 75% of the rain in the upper basin and 85% of the rain in the lower basin (Shrestha et al., 2015).

2.2. A brief overview of data extraction and its description

2.2.1. Groundwater storage anomalies (GWSA)

This research calculated the GWSA by subtracting the model-based TWSA $_{GLDAS}$ data from Satellite-based TWSA $_{GRACE}$ data (equation-1) (Sun et al., 2019). Many studies have used this method to derive GWSA in different world regions. (Leblanc et al., 2009; Rodell et al., 2007; Tiwari et al., 2009).

$$GWSA = TWSA_{GLDAS} - TWSA_{GRACE} \quad (1)$$

The Gravity Recovery and Climate Experiment (GRACE) twin satellite mission launched in 2002, which provided the global Terrestrial Water Storage anomalies (TWSA) over 15 years (2002–2017). The GRACE satellite mission collaborates with the US and German space agencies (NASA and GFZ). This study calculated the TWSA $_{GRACE}$ data from the monthly GRACE data products (Level-2 RL-05) at $1^\circ \times 1^\circ$ spatial resolution from January 2003 to December 2016. The monthly GRACE Datasets were obtained from the NASA Jet Propulsion Laboratory (JPL), the Center for Space Research (CSR) at the University of Austin-Texas, and the German Research Center for Geosciences (GFZ) research agencies (Dharpure et al., 2020). The GRACE data products (CSR, JPL, and GFZ) are available for free from "ftp://isdcftp.gfz-potsdam.de/grace/." GRACE Datasets have missing values for 17 months, and these values were completed using the means values before and after the missing months (Yang et al., 2017; Long et al., 2015). The following Eq. (2) represents the TWSA $_{GRACE}$ components (Bhanja et al., 2020):

$$TWSA_{GRACE} = GWSA + SMSA + SWSA + SWEA + CWSA \quad (2)$$

The GWSA is the groundwater storage, SMSA is soil moisture storage, SWSA is surface water storage, SWEA is snow water equivalent anomaly, and CWSA is canopy water storage.

The Global Land Data Assimilation System (GLDAS) is a project of Land Data Assimilation System (LDAS) and joint products of the National Aeronautics and Space Administration (NASA) Goddard Space Flight Center (GSFC), the National Centers of Environmental Prediction (NCEP), and the National Oceanic and Atmospheric Administration (NOAA) (Rodell et al., 2004). GLDAS provides optimal land surface states and fluxes by combining ground-based and satellite-based data observation. GLDAS uses land surface models (LSMs): Mosaic (Koster and Suarez, 1996), NOAH (Chen et al., 1996; Ek et al., 2003), Variable Infiltration Capacity (VIC) (Liang et al., 1994), and Community Land Model (CLM2.0) (Dai et al., 2003) to generate the global high-resolution (2.5° to 1 km) data (Dharpure et al., 2020; Rui and Beaudoing, 2020).

To estimate the monthly TWS_{GLDAS} (Total Water Storage) data with minimum bias, a summation of the monthly soil moisture (SM) layer, snow water equivalent (SWE), and canopy water storage (CWS) from the average of four GLDAS LSM datasets (with a spatial resolution of $1^\circ \times 1^\circ$) used during the period 2003–2016 (Yang et al., 2017 ; Ahmed and Abdelmohsen, 2018). Due to the lack of groundwater storage data in the LSMs dataset (Rodell et al., 2004; Dai et al., 2003), we consider that the surface water storage (SWS) data have minor contributions to the study area, so the SWS was neglected. Then the TWS_{GLDAS} data was converted into anomalies ($TWSA_{GLDAS}$) to derive the GWSA from Eq. (1) (Dharpure et al., 2020).

2.2.2. Potential evapotranspiration (PET)

The Global Data Assimilation System (GDAS) uses by NCEP/Global Forecast System (GFS) model to generate the operational global atmospheric data. GDAS assimilates a variety of meteorological data (surface observations, radiosonde data, buoy observations, radar observations, and aircraft reports) and satellite observations by using a multivariate approach and provides operational and global analyses every 6 h (four synoptic hours: 0000, 0600, 1200, and 1800 UTC) (Rodell et al., 2004). GDAS data are available through NOAA National Operational Model Archive and Distribution System (NOMADS). The potential evapotranspiration (PET) data was estimated from GDAS's climate parameter data (as air temperature, atmospheric pressure, wind speed, relative humidity, incoming and outgoing shortwave, and longwave radiation) using the Penman-Monteith equation (Allen et al., 2006; Shuttlewor, 1992) for every 6 h. The daily PET data with a spatial resolution of 1° × 1° was acquired from 2003 to 2016 (Table 1) from the USGS website https://earlywarning.usgs.gov/fews/product/81.

2.2.3. Tropical rainfall measuring mission (TRMM) precipitation

TRMM satellite was launched in 1997 by collaboration between NASA and the Japanese Aerospace Exploration Agency (JAXA). TRMM was the first mission to measure rain in the tropics and subtropics regions using microwave, infrared and visible sensors. Rain gauge data and ground-based radars complement satellite observations to validate satellite precipitation estimation techniques (George J. Huffman et al., 2007). Comparison of observational and TRMM data shows good agreement between them, and several types of the research reported good accuracy (Jia et al., 2011; Khan et al., 2018; Yang et al., 2017). This study acquired the precipitation (P) data from the TRMM 3B43 monthly research version 7 (TRMM_3B43_7) in HDF formats at the spatial resolution of 0.25° × 0.25° over the GRB during 2003–2016 (Table 1). The TRMM_3B43_7 data products were acquired from the NASA EARTHDATA website (https://disc.gsfc.nasa.gov/datasets).

2.2.4. Moderate resolution imaging spectroradiometer (MODIS) LST

The MODIS instrument operates aboard the Terra and Aqua satellites, which Terra launched in 1999 and Aqua launched in 2002 by NASA. MODIS instruments view the entire Earth's surface every 1 to 2 days and acquire data in 36 spectral bands with an overpass at around 10:30 am (descending) for Terra and 1:30 pm (ascending) for Aqua. The MODIS observations describe features of the land, oceans, and atmosphere. In this research, MODIS land surface temperature (LST) Monthly Level 3 Global products, including MOD11C3 (Terra) and MYD11C3 (Aqua) version 6 at the spatial resolution of 0.05° × 0.05°, were used (Table 1). MODIS data were obtained from products on the NASA NASA EARTHDATA website (https://earthdata.nasa.gov/) (Dharpure et al., 2020).

Table 1
The satellite-based and model-based data used duration 2003–2016.

Satellite /Model Database	Variables	Agencies/Model/ Product (version)	Spatial-temporal resolution
GLDAS- Model Database	$TWSA_{GLDAS}$ (averaging Mosaic, NOAH, VIC, CLM)	MOSAIC (V001)	1° × 1°, Monthly
		CLM (V001)	1° × 1°, Monthly
		VIC (V001)	1° × 1°, Monthly
		NOAH (V001)	1° × 1°, Monthly
GRACE Satellite Database	$TWSA_{GRACE}$ (averaging GFZ, CSR, JPL)	CSR (RL05)	1° × 1°, Monthly
		JPL (RL05)	1° × 1°, Monthly
		GFZ (RL05)	1° × 1°, Monthly
TRMM Satellite Database	P	3B43 (V7)	0.25° × 0.25°, Daily
GDAS Model Database	PET	SPEIbase (V2.4)	1° * 1°, Daily
MODIS Satellite Database	LST	MOD11C3 (V6)	0.05° × 0.05°, Monthly
		MYD11C3 (V6)	0.05° × 0.05°, Monthly
ERA5-LAND Model Database	WS, Runoff, Air Temp, SWN, LWN, ET, and NR	ERA (V5)	0.1° × 0.1, Monthly

2.2.5. ECMWF Reanalysis V5 - Land (ERA5-LAND) variables

The European Centre for Medium-Range Weather Forecasts (ECMWF) generates an improved global dataset for the land component of the fifth generation of European Reanalysis (ERA5-Land). The ERA5-Land dataset is hourly high-resolution (0.1° × 0.1°; 9 km) surface variables that describe the water and energy cycles overland from 1981 to 2–3 months before the present (Jamei et al., 2020; Muñoz-Sabater et al., 2021). The ERA5-Land Monthly averaged data were employed in this study, including; Wind Speed (WS), Runoff, Air Temperature at 2 m (Air Temp), Surface net solar radiation (or shortwave radiation) (SWN), Surface net thermal radiation (or longwave radiation) (LWN), Evapotranspiration (ET), and net radiation (NR) data from Copernicus website (https://cds.climate.copernicus.eu/) (Table 1). ET data is available in the ERA5-Land variables named Total Evaporation, which includes the values of evaporation and transpiration. NR was obtained from the sum of the SWN and the LWN (Elbeltagi et al., 2021Xu et al., 2003).

2.2.6. Calculation of CTEI index

As mentioned in the previous section, the CTEI index was developed by (Dharpure et al., 2020) as a novel drought index, which describes meteorological, hydrological, and agricultural drought. The CTEI is a drought index designed to identify and monitor all types of droughts with the combined impacts of precipitation, water demand (potential evapotranspiration), and the Terrestrial Water Storage Anomaly (TWSA). The CTEI is calculated using meteorological parameters and satellite-based data. The CTEI was modeled using a number of 168 series of data sets, including the satellite-based $TWSA_{GRACE}$ data and meteorological variables (P and PET) (Dharpure et al., 2020) from 2003 to 2016 (Table 1. The first step calculates the difference (D) between the meteorological variables P and PET for the month i^{th} using equation (3) (Vicente-Serrano et al., 2010).

$$D_i = P_i - PET_i \tag{3}$$

The monthly differences anomaly (D_{Ai}) time series was calculated from equation (4) (Sinha et al., 2019):

$$D_{Ai} = D_i - D_m \tag{4}$$

where D_m is the mean value of a baseline period of January 2004 to December 2009 (Dharpure et al., 2020), then the climatology of D_A and $TWSA_{GRACE}$ are obtained from the GRACE deficit method (Thomas et al., n.d.). The climatology of all 168 months from January 2003 to December 2016 for the D_A and $TWSA_{GRACE}$ time series was calculated by monthly averaging the D_A and $TWSA_{GRACE}$ values, respectively. To calculate the D_A and $TWSA_{GRACE}$ time series residuals, the monthly climatology of D_A and $TWSA_{GRACE}$ were subtracted from each month of D_A and $TWSA_{GRACE}$, respectively. The $TWSA_{GRACE}$ residual was added to the D_A residual. The combined water storage anomalies (CWSA) were obtained, representing a net deviation in water storage volume based on seasonal variability. The CWSA was normalized using Equation (5) and, the $CWSA_m$ and $CWSA_\sigma$ are the means and standard deviation of CWSA, respectively, for each month (Dharpure et al., 2020).

$$CTEI = \frac{CWSA_i - \mathrm{CWSA}_m}{CWSA_\sigma} \tag{5}$$

The CTEI index is indeed the combined terrestrial normalized net deviation in water storage volumes (Dharpure et al., 2020). The variation of all the input features and CTEI are shown in Fig. 2.

2.2.7. Statistical data description

In this study, a number of 168 monthly data sets was collected from combined hydro-metrological and satellite data, as aforementioned in the previous section. Table 2 demonstrates the statistical indices of all considered variables in modeling CTEI. According to Table 2, the SW (32.75), NR (26.39), and LWR (24.51) have the maximum standard deviation among all variables. Besides, the maximum skewness and kurtosis belong to Runoff (1.356) and LST (-1.099), respectively. However, the range of skewness and kurtosis is limited within [-1.2, 1.2], which implies that the distribution of the entire implemented variable is closed to normal.

2.3. Theoretical background

2.3.1. Relief-based feature selection

The feature selecting process is a mechanism to reduce the dimensionality of data sets in the classification and regression tasks and eliminate the redundant and irrelevant features which have a low effect on the target of the models. This mechanism can reduce the computational cost and time-consuming time in the training stage, decrease overfitting, reduce complexity, and improve acceptable accuracy based on minimum features. The feature selection (FS) methods used in ML applications are categorized into three types: filter, wrapper, and embedded. Relief algorithm is one of the most popular and simple instance-based learning (FS), which, for the first time, is formulated by Kira and Rendell (Kira and Rendell, 1992) and advanced by Kononenko (Kononenko, 1994). As an iterative non-deterministic procedure, the Relief approach randomly selects a subset of training samples in the feature space to capture the degree of relevancy between selected features and the target. The main idea of this method is to determine the importance weight of each selected feature in the sampled instance to evaluate the distinguishing ability among the class labels.

Further importance weight (ω_s) of a considered feature shows that it has more chance to be chosen as the input to predict the target feature (Malik and Yadav, 2021). In this approach, an instance is randomly selected from the training set. In each instance subsets, the closest distance between the desired feature and the target is determined with k-nearest neighbors, and the maximum weight value is allocated to it. The Euclidean distance metric is applied to find the nearest Hit and nearest Miss instances for the examined samples as(Amjady and Keynia, 2009):

$$d_{mn} = \sqrt{x_m{}^2 + x_n{}^2 - 2x_n x_m} \tag{6}$$

where d_{mn} is the Euclidean distance between two sampled vectors (x_m and x_n), it should be mentioned that the nearest Hit and nearest Miss are defined as two samples that have the smallest Euclidean distance with same and opposite classes, respectively. The algorithm of relief FS can be expressed as(Robnik-Šikonja and Kononenko, 2003):

1. Initiate all feature weights: $\omega_{s,i} = 0$
2. Iteratively choose a random instance with specific features and assume the number of neighbor nearest samples k
3. Finding the k-nearest for each class by Eq.(6) by random sampling a case from the data
4. Updating the weight of the i^{th} feature for each random instance using the following formula:

$$\omega_{s,i} = \omega_{s,i} - (x_i - nearHit_i)^2 + (x_i - nearMis_i)^2 \tag{7}$$

5. Standardize the weight score (ω_s) values, average the updated weights in all iterations, and achieve the final weight value. As a rule of thumb, the value of k can be obtained based on the number of data under training (Amjady and Keynia, 2009),

$$k = Round(log_2(N)) \tag{8}$$

2.3.2. Least square support vector regression (LSSVR)

SVR is one of the supervised learning techniques in nonlinear estimation problems (Cortes and Vlagimir, 1995). Function estimation in SVR is based on linear data classification, and the goal is to find a line that allows maximum separation. One of the primary problems of the SVR algorithm is the high computational cost and complexity of large-

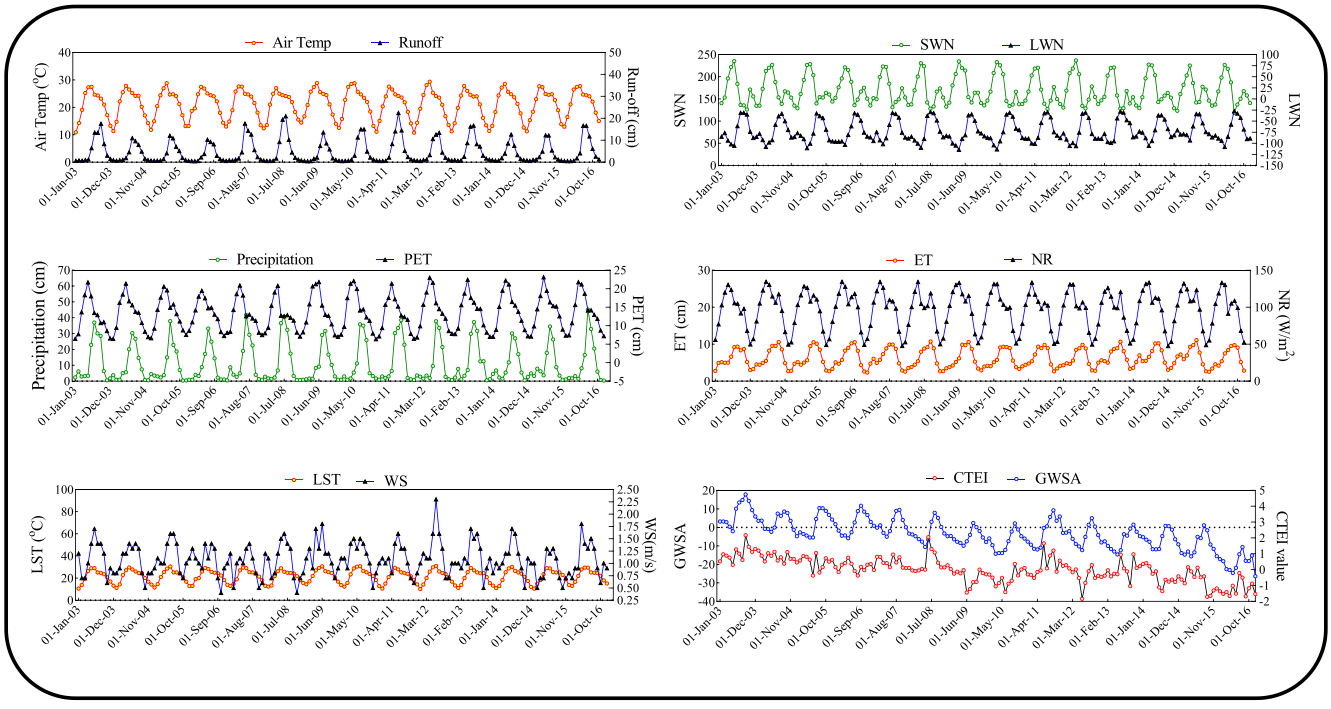

Fig. 2. The variation of input and output features associated with monthly CTEI simulation.

Table 2
Descriptive statistics of all collected variables.

Variables	Minimum	Maximum	Mean	Std. Deviation	Skewness	Kurtosis
GWSA	−26.420	17.810	−3.496	8.302	−0.105	−0.034
P	0.400	45.200	10.780	12.240	1.164	−0.039
LST	10.300	31.000	21.620	5.807	−0.337	−1.099
WS	0.400	2.300	1.077	0.331	0.328	0.198
ET	2.320	11.070	6.225	2.511	0.262	−1.295
Runoff	0.470	22.440	4.657	5.255	1.356	0.846
Air Temp	10.750	29.320	21.160	5.217	−0.447	−1.083
NR	47.700	134.400	96.000	26.390	−0.421	−1.055
SWN	118.400	236.700	168.900	32.750	0.588	−0.967
LWN	−114.000	−27.040	−72.920	24.510	0.526	−1.005
PET	6.380	23.130	13.340	4.720	0.296	−0.993
CTEI	−1.840	2.170	0.000	0.785	−0.127	−0.067

scale problems because it uses the convex quadratic programming method (Naseri et al., n.d.). To increase accuracy and reduce complexity, (Suykens and Vandewalle, 2000) developed the LSSVR model, which uses linear equations. This model uses simple linear equations to solve problems, effectively reducing the algorithm's complexity and increasing the computational speed compared to the SVM model. The regression function used to estimate the problems is as follows (Jamei et al., 2021).

$$y(x_i) = w^T.\phi(x_i) + b \tag{9}$$

where $\phi(x_i)$ is the nonlinear mapping of the inputs in the feature space with high dimensions. Parameters w and b are the values of weights and bias of the regression function, respectively, which are determined by minimizing the objective function in the following Eq. (10):

$$Min_{w,e,b}j(w,e) = \frac{1}{2}w^T.w + \frac{\gamma}{2}\sum_{i=1}^{N} e_i^2 \tag{10}$$

With constraints:

$$y_i = w^T.\phi(x_i) + b + e_i \quad i = 1, 2, \cdots, N \tag{11}$$

where γ is the parameter regulating the error section and e_i is the error of the training data. Finally, the LSSVR model estimation function is defined as the following relation:

$$y(x) = \sum_{i=1}^{N} a_i K(x_i, x_j) + b \tag{12}$$

In the above relation $K(x_i, x_j)$ is called the kernel function, based on Eq. (13), is introduced by creating an internal multiplication in the feature space.

$$K(x_i, x_j) = \langle \phi(x_i).\phi(x_j) \rangle \quad i,j = 1, 2, \cdots, N \tag{13}$$

The kernel functions studied in the present study included Linear, polynomial, and Radial Basis Function (RBF).

2.3.3. Artificial neural network

ANN is a computational method inspired by the human nervous system that can communicate precisely between inputs and outputs (Haykin, 2009). This study used the multilayer perceptron (MLP) approach with three input layers, hidden and output. MLP includes Feed-Forward Networks with Back Propagation training algorithm (Coulibaly et al., 2011). In each layer, a number of neurons are used as processor units and also an activation function. The computational output of each layer is transferred to the next layer. In this study, the stimulus functions and the number of hidden layer neurons were selected based on trial and error. The minimum error value for the hidden layer and the output included sigmoid tangent and linear, respectively. The mathematical model of a neural network can be summarized as follows (Haykin, 2009):

$$\widehat{y_k} = f_0\left[\sum_{j=1}^{m} w_{kj}.f_h\left(\sum_{i=1}^{n} w_{ij}x_i + w_{j0}\right) + w_{k0}\right] \tag{14}$$

where n is the total number of neurons in the input layer, m is the total number of neurons in the hidden layer, k is the total number of neurons in the output layer, f_0 is activation function at the output layer, f_h is activation function in the hidden layer, w_{j0} is bias weight of the j^{th} neuron in the hidden layer, w_{ji} is the weight of the i^{th} neuron in the hidden layer, w_{k0} is the bias of the k^{th} neuron in the output layer and w_{kj} is the weight of the j^{th} layer in the output layer. The value of w_{j0}, w_{ji},w_{k0} and w_{kj} is determined through the learning process. Fig. 3 demonstrated the structure of LSSVR and ANN models.

2.3.4. Whale optimization algorithm (WOA) – ANN

WOA is a meta-heuristic approach that uses a population of search agents (Mirjalili and Lewis, 2016). Humpback whales' nature inspires the WOA and social behavior, explored and exploited based on a bubble-net feeding propensity strategy. Avoiding local optimal points with an integrated adaptive technique is one of the algorithm's capabilities to find the optimal solution with the least loss of computational time. The three main steps of the algorithm include search, surround, and prey attack. In the WOA mathematical model, first, a set of walls is randomly determined, and then the position of the whales in each iteration changes according to the problem conditions. Each whale will be a candidate solution to the problem, and ultimately the optimal solution will be based on the least prediction error. In the WOA algorithm, the prey position is the best (optimal global answer). The position of the whales is updated based on the prey according to the following Equation:

$$\overrightarrow{Y}(t+1) = \overrightarrow{Y}_p(t) - \overrightarrow{B}.\left|\overrightarrow{D}.\overrightarrow{Y_p}(t) - \overrightarrow{Y}(t)\right| \tag{15}$$

where $\overrightarrow{Y}_p(t)$ and $\overrightarrow{Y}(t)$ are prey and whale position vectors in t[th] iteration, B and D are coefficient vectors according to the following Equation:

$$\overrightarrow{B} = 2\overrightarrow{b}.\overrightarrow{r_1} - \overrightarrow{b} \tag{16}$$

$$\overrightarrow{D} = 2.\overrightarrow{r_2} \tag{17}$$

in which $\overrightarrow{b}$ is linearly reduced from 2 to zero during the algorithm process and $\overrightarrow{r}$ is a random vector with values in the range [0, 1].

After the surrounded of the prey, the attack begins based on the bubble-net approach. To imitate the spiral motion of whales in attack, the spiral Equation, which shows the distance between the position of the whale and the prey, is used as follows:

$$\overrightarrow{Y}(t+1) = \overrightarrow{E}.e^{zI}.cos(2\pi I) + \overrightarrow{Y}_p(t) \tag{18}$$

where z is a constant value and represents the motion of the logarithmic

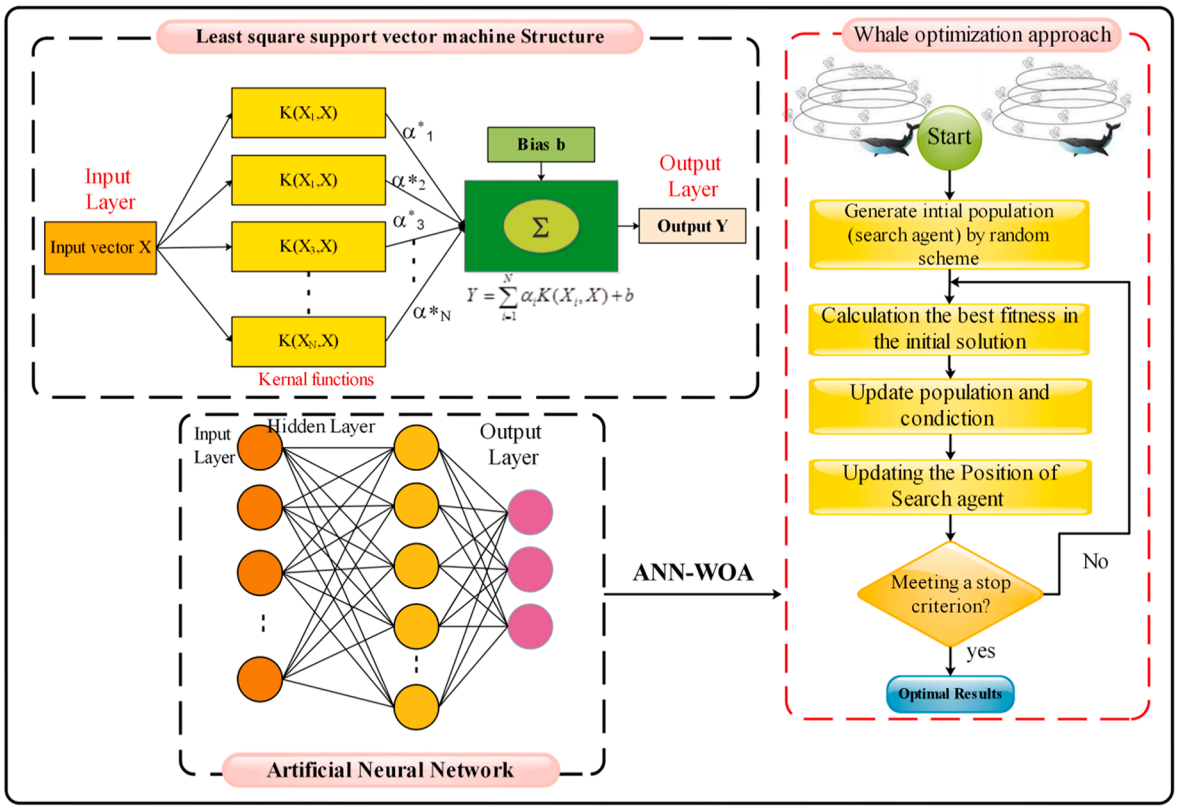

Fig. 3. Schematic structure of the ANN and SVM approaches.

spiral, *I* is a random value in the interval [−1, 1], and E is the distance between the whale and the prey as follows:

$$E = \left|\vec{Y}_p(t) - \vec{Y}(t)\right| \tag{19}$$

where $\vec{Y}_p(t)$ and $\vec{Y}(t)$ are prey and whale position vectors. More information and details of WOA are reported by (Mirjalili and Lewis, 2016). The flowchart of the WOA method is depicted in Fig. 3.

In ANN, the Back Propagation algorithm is used to adjust the values of the weights and biases of each neuron so that the difference between the observed and predicted values is reduced. The weight and bias of each neuron have the most significant effect on the error rate of estimating the target variable (Mirjalili et al., 2012; Zhang et al., 2007). In this study, the WOA algorithm is used for optimizing the weight and bias of each neuron. The weight and bias change with each iteration, and WOA moves toward an optimal global solution by limiting the decision space. Avoiding WOA from over-fitting and not being trapped in local optimization is one of the differences between network training with WOA versus backward propagation algorithms. The condition for stopping the process is to reach the maximum number of iterations or a certain amount of error. Finally, the optimal weights and biases of WOA-ANN are determined and evaluated with the data of the test section. In this study, using trial and error, the initial population and number of iterations were selected as 20 and 1500, respectively.

2.3.5. Models evaluation metrics

The results of the models used in this study were evaluated with five statistical indicators, which include the following: The root mean square error (RMSE), the mean absolute error (MAE), Uncertainty with 95% a confidence level ($U_{95\%}$), Willmott Index (WI), and the correlation coefficient (R). The equations of the mentioned indicators are as follows (Karbasi et al., 2021a; Malik et al., 2021b):

$$R = \frac{\sum_{i=1}^{n}(M_i - \overline{M})(P_i - \overline{P})}{\sqrt{\left[\sum_{i=1}^{n}(M_i - \overline{M})^2\right]\left[\sum_{i=1}^{n}(P_i - \overline{P})^2\right]}} \tag{20}$$

$$RMSE = \sqrt{\frac{\sum_{i=1}^{n}(M_i - P_i)^2}{N}} \tag{21}$$

$$MAE = \frac{1}{n}\sum_{i=1}^{n}|M_i - P_i| \tag{22}$$

$$U_{95\%} = 1.96\sqrt{\left(SD_e^2 + RMSE^2\right)} \tag{23}$$

$$\mathrm{WI} = 1 - \frac{\sum_{i=1}^{\mathrm{N}}(M_i - \mathrm{P_i})^2}{\sum_{i=1}^{\mathrm{N}}(|\mathrm{P_i} - \overline{M}| + |\mathrm{M_i} - \overline{M}|)^2} \tag{24}$$

where n is the number of observations in the data set, M_i and P_i are the measured and predicted monthly CTEI values, respectively, $\overline{M}$ and $\overline{P}$ are the average monthly CTEI in the measured and predicted data, respectively, and SD_e is the standard deviation of the error (difference between measured and predicted values). The road map of all stages of the modeling process of monthly CTEI is illustrated in Fig. 4.

3. Results and discussion

3.1. Best input combination assessment

Predictability exploring the monthly CTEI based on satellite and metrological data with WOA-ANN was adopted along with the other standalone ML approaches comprised of LSSVR (with linear, polynomial, and RBF kernel functions) and ANN models with different

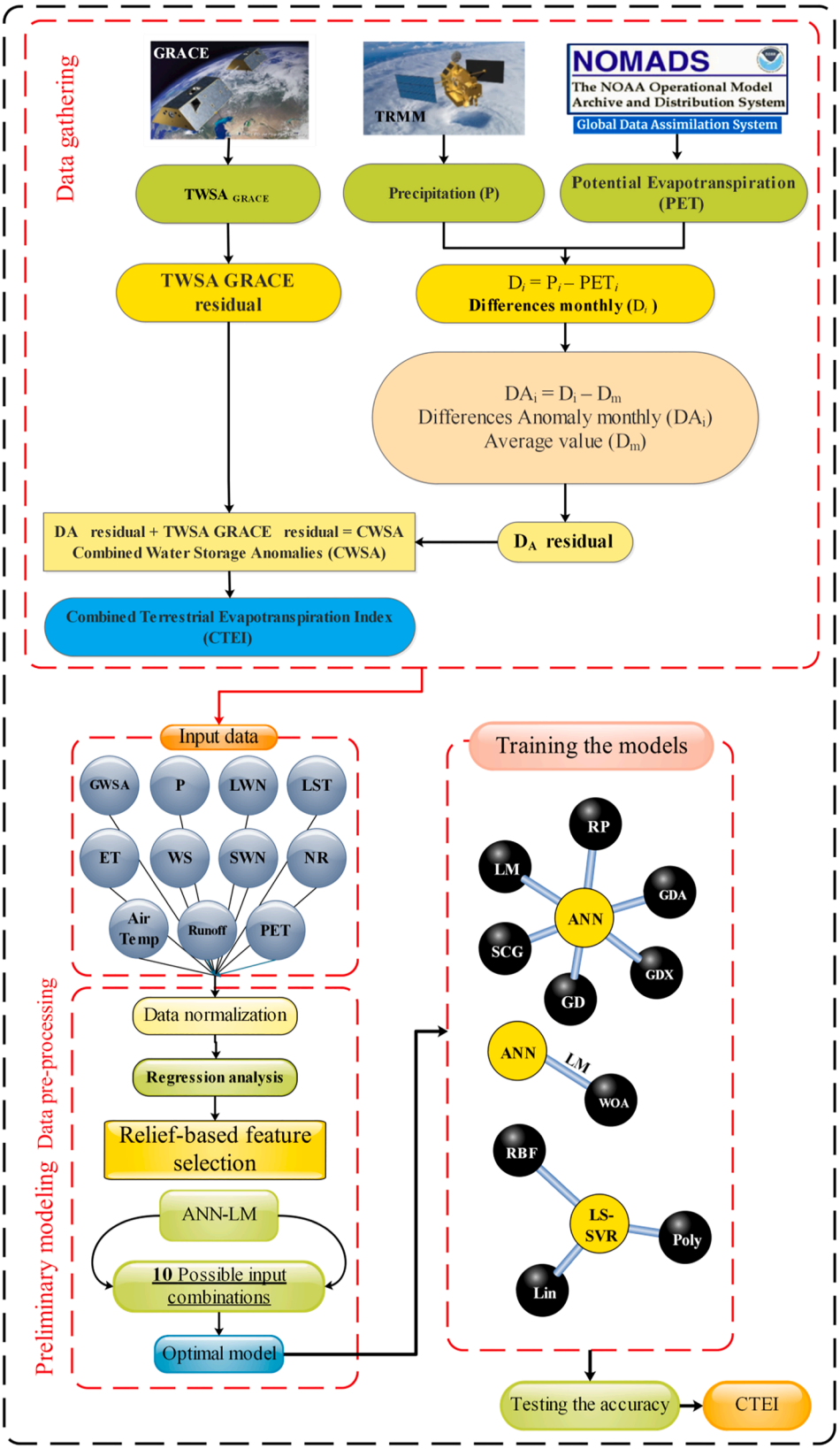

Fig. 4. The road map of modeling the monthly CTEI using three AI based approaches.

training algorithms. At the first modeling stage, the best input combination was sought using data preprocessing and an elementary simulation using ANN models. Regarding Fig. 5, the Pearson correlation coefficient between CTEI and all features demonstrates that the GWSA by the highest linear correlation coefficient (r_P=0.66), Run-off (r_P=0.18), and P (r_P=0.16) are the most effective features in the modeling monthly CTEI. Besides, ET (r_P=0.04), WS (r_P=0.66), NR (r_P=−0.07), LST (r_P=−0.08), and air Temp (r_P=−0.08) on account of

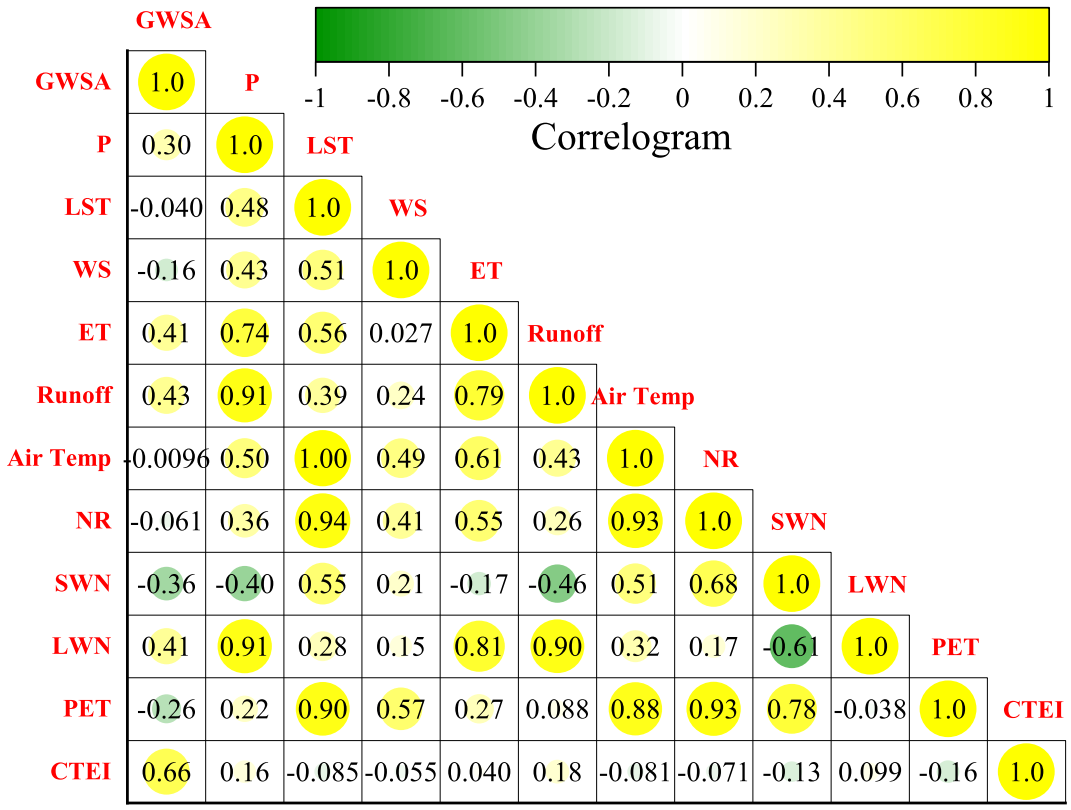

Fig. 5. The matrix of correlation between all features.

the lowest linear dependency seem to have less impact on the value of the index of CTEI. Although, the real importance impact of each variable on target can be specified after a comprehensive assessment using a robust Fs approach. For this aim, relief-algorithm FS was employed to reliably identify the best efficient input combinations. According to Fig. 6, the performed analysis using relief-algorithm FS demonstrated that GWSA (ω_s=0.0442), Runoff (ω_s=0.0147), P (ω_s=0.0093), and PET (ω_s=0.0092) are the most influential features for estimation of monthly CTEI. It has a reasonably good agreement with the Pearson correlation analysis. Concerning the analysis mentioned above, ten superior input combinations were selected among all possible ones which GWSA, on account of higher impact, was imposed in them.Fig. 7.

Furthermore, the Runoff, P, and PET features were arranged into selective input combinations based on their importance weight. Table 3 reported the input combinations obtained by the relief FS. The optimum input combination was examined using ANN models and Levenberg–Marquardt (LM) triaging function in the next stage. This function is commonly recognized as the most option for developing ANN models (Vidyarthi et al., n.d.). For this purpose, ten input combinations were evaluated using numerous statistical criteria tabulating in Table 4. The results demonstrated that the Combo 6, including the GWSA, precipitation (P), air-Temp, NR, SWN, LWN, and PET on account of highest (R = 0.885, WI = 0.935) and lowest (RMSE = 0.330, MAE = 0.266, and U_{95}% = 0.910), has the superior predictive performance among all combinations followed by Combo 8 (R = 0.840, WI = 0.911, RMSE = 0.386, and U_{95}% = 1.070) in the testing phase. Fig. 7 illustrates the variation of R, RMSE, and $U_{95\%}$ for understudy combinations, and the features number for each combination is specified on the right side of plots (Yellow circle). The variation trend of R proved that the combinations with more input features could not achieve promising outcomes. Fig. 8 depicted the box plot of predicted and measured CTEI distribution for whole datasets in all the combinations. Fig. 8 ascertains that Combo 6, Combo 8, and Combo 5 have the best agreement with measured CTEI values. The statistical indicators owing to Combo 1, Combo 2, and Combo 3 (in Table 4) showed notable performance in training and a disappointing performance in the testing stage, confirming the under/overestimation in those combinations. Hereinafter, the Combo 6 is considered the benchmark for evaluating the proposed AI techniques in predicting CTEI.

3.2. Application of optimum combination and models analysis

After identifying the optimum candidate input combination (Combo 6), six ANN models based on different training functions comprised of LM, SCG, RP, GDX, DDA, and GD were designed to find the best prediction and most efficient training function. Besides, the optimum training function was employed in WOA-ANN as the main novelty of the current research. Three LSSVR models using linear, polynomial, and RBF kernel functions were examined to validate the WOA-ANN model better. Table 5 lists the statistical evaluation criteria and setting parameters for each model. Precisely assessment of the ANN models demonstrated that ANN_1 model by LM training function and structure of 7-3-1 in terms of (R = 0.884, RMSE = 0.319, MBE = 0.235, and $U_{95\%}$ = 0.885) in training and (R = 0.885, RMSE = 0.330, and $U_{95\%}$ = 0.910) in the testing stage yielded the most accurate prediction of monthly CTEI in comparison with the other ANN models. Also, the ANN_5 using RP function was the best second metric in the testing phase (R = 0.857, RMSE = 0.377, and $U_{95\%}$ = 1.047) stood at the second rank. Fig. 9 depicted the degree of consistency between observed and predicted CTEI values using ANN models. It was apparent from Fig. 9 that the ANN_1 model using the LM training function had the best agreement with the measured CTEI values, and the LM function was ascertained as the selective option to achieve the best predictive models followed by PR, and GDA functions, respectively. A closer assessment of the scatter plots shows that the ANN models for CTEI > 0 led to more promising outcomes, and the predictive monthly CTEI values were more relative to the best line (45° line).

In the next validation case, Fig. 10 demonstrates the probability distribution function (PDF) of all ANN models and measured monthly

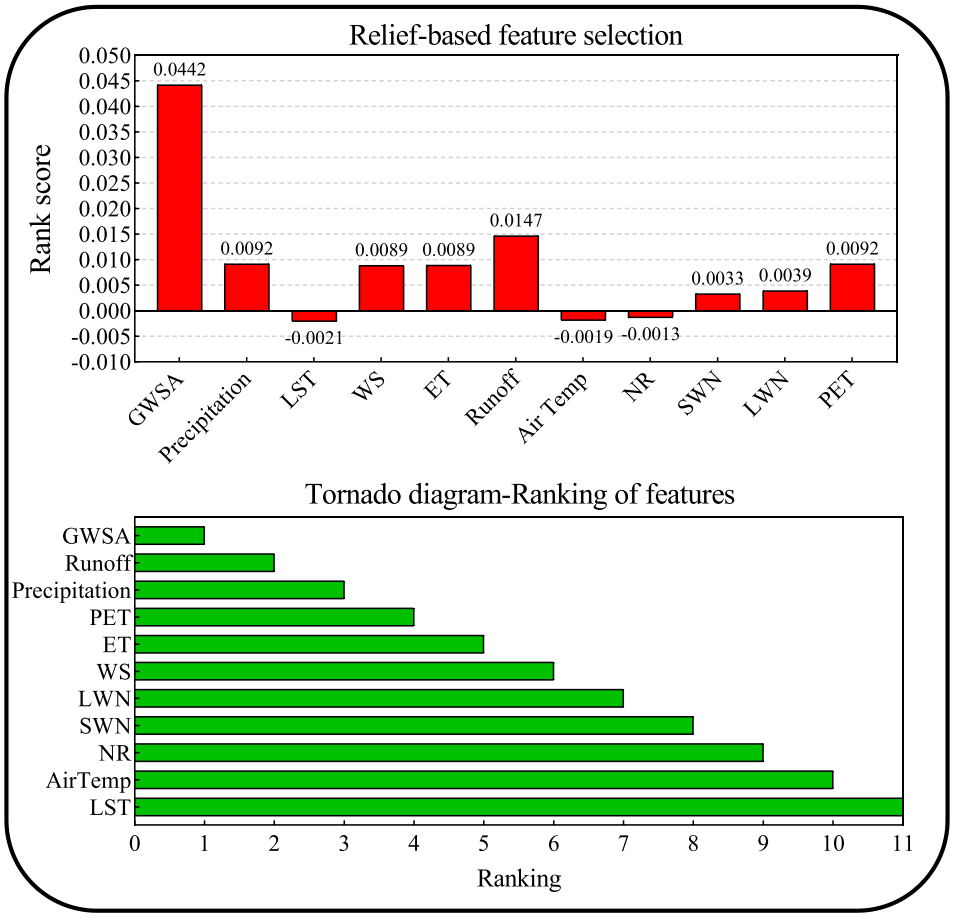

Fig. 6. The outcomes of relief-based feature selection (a) Rank score of all features (B) the tornado diagram of feature ranking importance.

CTEI values, which confirm that LM and RP had superior predictive performance among all the models, respectively.

3.3. Assessment of WOA-ANN and LSSVR models

The hybrid ANN (LM) model integrated with the WOA scheme yields better results than the standalone ANN method. Thus, to have a more detailed inspection of the provided soft computing predictive models, the WOA-ANN using the LM training function was sought with the LSSVR approach applying three kernel functions and the ANN_1 model. According to Table 5, the model of $LSSVR_3$ is based on RBF kernel function in terms of (R = 0.8390, RMSE = 0.373, $U_{95\%}$ = 1.035) in training and (R = 0.8854, RMSE = 0.342, $U_{95\%}$ = 0.944) in testing modes performed in better accuracy level in comparison with the other inspected kernel function. Furthermore, it is clear that the WOA-ANN model on account of the highest (R = 0.939 and WI = 0.969) and lowest error metrics (RMSE = 0.241 and MAE = 0.185) is significantly superior to the $LSSVR_3$ and ANN_1 approaches by a correlation coefficient of 0.8854 and 0.8847, respectively in the testing stage. In addition, Fig. 11 reported that the WOA-ANN model has fewer scattered estimates than three LSSVR models and can yield promising precision $CTEI > -1$.

3.4. Comparative study between developed AI models and discussion

In this section, further insight into proposed models was addressed by quantitative comparison between the obtained results. As mentioned before in the previous discussion, the predicted monthly CTEI using the WOA-ANN model in terms of (R = 0.939 and RMSE = 0.2406) had considerably better agreement with the measured values than those of $LSSVR_3$ (R = 0.8854 and RMSE = 0.3416) and ANN_1(R = 0.8847 and RMSE = 0.3304) in the testing phase. Fig. 12 explains the PDF of WOA-ANN, LSSVRs, and ANN_1 approaches versus the measured CTEI value for all the datasets. A careful assessment of the violin plots displays that WOA-ANN and ANN_1 models regarding the best consistency with measured CTEI yield the more reliable and accurate prediction results, respectively, and $LSSVR_1$ has the worth accuracy among all compared models.

Fig. 13 exhibits the Taylor diagrams of ANN_1, $LSSVR_3$, and WOA-ANN models in the optimum input combination for both training and testing phases. The physical distance of each model representation to the target (observed) point showed that WOA-ANN owing to smallest distance identified as the best superior predictive model, and ANN_1, regarding the better performance and smaller diagnostic criteria in comparison with $LSSVR_3$, stood in the second rank of the understudy models in predicting the CTEI.

The expected physical trend of each understudy model was examined to evaluate their ability to capture the nonlinear behavior of the monthly CTEI datasets for both training and testing phases in Fig. 14 which the pick intervals for better judgment are magnified below each plot. Examination of the results showed that the WOA-ANN paradigm successfully captures the peak points in the trend of monthly CTEI datasets for both training and testing stages, and ANN_1 could get better efficiency than LSSVRs models in predicting process.

In the next evaluation stage, the error analyses were performed on the basis of the relative deviation (RD) and cumulative frequency of absolute relative deviation (CFARD). Fig. 15 depicted the PDF (Left) and scattered (Right) RD for all selective models in training and testing modes. The WOA-ANN by RD-range of ($-343\% \leqslant RD \leqslant 551.6\%$) yields the least under/overestimation and highest accuracy in comparison with $LSSVR_3$ and ANN_1 models by RD-range of ($-928\% \leqslant RD \leqslant 802.4\%$) and

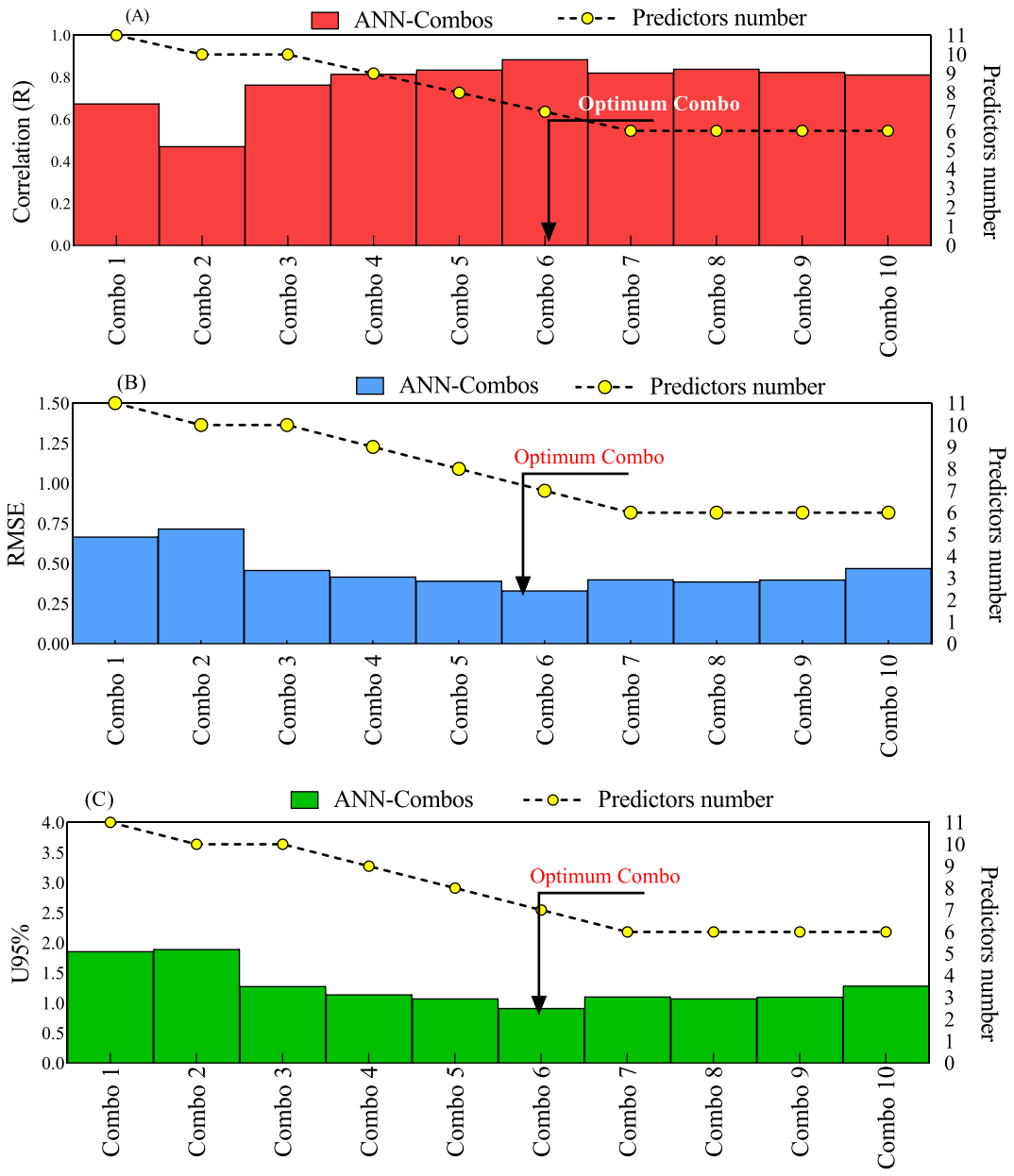

Fig. 7. The variation of R, RMSE, and $U_{95\%}$ for all possible input combination.

Table 3
The input combinations arrangement for seeking the best combination.

Models	Input Combinations	Inputs number
Combo 1	GWSA, P, LST, WS, ET, Runoff, Air Temp, NR, SWN, LWN, PET	11
Combo 2	GWSA, LST, WS, ET, Runoff, Air Temp, NR, SWN, LWN, PET	10
Combo 3	GWSA, P, WS, ET, Runoff, Air Temp, NR, SWN, LWN, PET	10
Combo 4	GWSA, P, ET, Runoff, Air Temp, NR, SWN, LWN, PET	9
Combo 5	GWSA, P, Runoff, Air Temp, NR, SWN, LWN, PET	8
Combo 6	GWSA, P, Air Temp, NR, SWN, LWN, PET	7
Combo 7	GWSA, P, NR, SWN, LWN, PET	6
Combo 8	GWSA, P, Air Temp, SWN, LWN, PET	6
Combo 9	GWSA, P, Air Temp, NR, LWN, PET	6
Combo 10	GWSA, P, Air Temp, NR, SWN, PET	6

(−771.55%⩽*RD*⩽1150.5%), respectively. It is noteworthy that all the provided AI based models in a range of (−0.5⩽*CTEI*⩽0.5) led to the most unreliability in estimating the CTEI values.

Finally, Fig. 16 demonstrated the pie plots of CFARD values for three selective AI predictors. The pie plots illustrate that about 30% of whole predicted data pints by WOA-ANN have an absolute relative deviation (ARD%) less than 10%. In contrast, only 17.34% and 14% of values predicted by ANN_1 and $LSSVR_3$ have ARD% less than 5%, respectively. Besides, 45.5% of whole predicted data has ARD% values more than 20%, whereas 71.26% and 72.46% of values predicted by ANN_1 and $LSSVR_3$ yield the ARD % more than 20%, respectively. Overall, it can conclusively be introduced the WOA-ANN as the superior model and for prediction of CTEI followed by the ANN_1 and $LSSVR_3$, respectively.

The outcomes of this research clearly exhibit that the WOA-ANN, for the similar basin and datasets, in terms of (R = 0.9391 and RMSE = 0.2406) is superior and more accurate than the best-provided models (R = 0.905 and RMSE = 0.33) in the study of Elbetagi et al.(Elbeltagi et al., 2021). In the optimum scenario in this research, Combo 6 using seven-

Table 4
The outcome of the best input combination selection using the ANN model.

Combo	Neurons	Mode	R	WI	RMSE	MAE	U_{95}%
Combo 1	2	Training	0.9422	0.9696	0.2284	0.1758	0.6344
		Testing	0.6748	0.7961	0.6660	0.4529	1.8551
Combo 2	2	Training	0.8969	0.9432	0.3016	0.2293	0.8377
		Testing	0.4712	0.6332	0.7171	0.5921	1.8891
Combo 3	2	Training	0.9197	0.9568	0.2678	0.2149	0.7438
		Testing	0.7636	0.8664	0.4578	0.3841	1.2745
Combo 4	2	Training	0.8395	0.9081	0.3705	0.2695	1.0292
		Testing	0.8153	0.8881	0.4167	0.3308	1.1365
Combo 5	2	Training	0.8206	0.8951	0.3898	0.2776	1.0825
		Testing	0.8360	0.8952	0.3902	0.2974	1.0705
Combo 6	**3**	**Training**	**0.8840**	**0.9354**	**0.3188**	**0.2353**	**0.8853**
		Testing	**0.8847**	**0.9354**	**0.3304**	**0.2658**	**0.9096**
Combo 7	3	Training	0.8342	0.9048	0.3760	0.2637	1.0444
		Testing	0.8217	0.8900	0.3997	0.3208	1.1023
Combo 8	3	Training	0.8835	0.9352	0.3195	0.2437	0.8874
		Testing	0.8400	0.9111	0.3863	0.3043	1.0697
Combo 9	2	Training	0.8286	0.9006	0.3818	0.2982	1.0603
		Testing	0.8248	0.8948	0.3992	0.3301	1.0987
Combo 10	4	Training	0.9102	0.9510	0.2825	0.1902	0.7845
		Testing	0.8120	0.8871	0.4706	0.3501	1.2822

The bold item indicates the optimum combination.

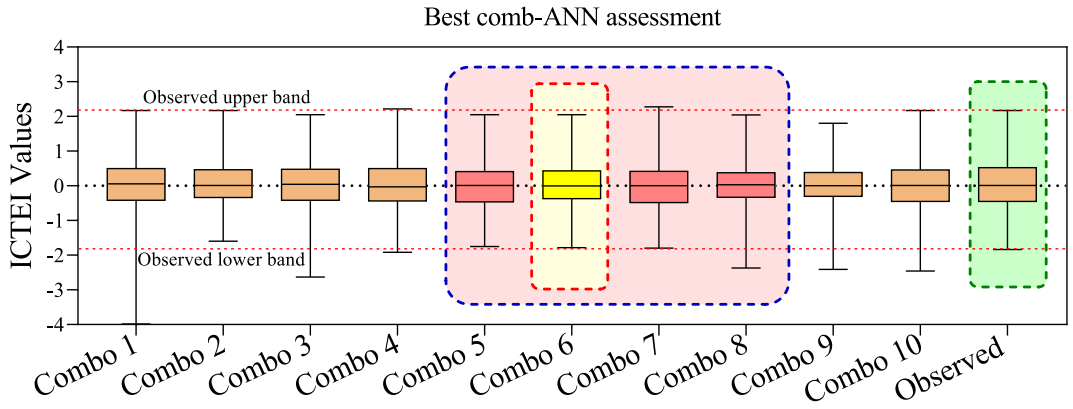

Fig. 8. The comparison between the measured predicted monthly CTEI values in the best selection input combination process.

Table 5
The statistical evaluation indices for all provided models in the best input combination.

Models	Functions Algorithm	Structure	Mode	R	WI	RMSE	MAE	U95%
ANN1	LM	7-3-1	Training	0.8840	0.9354	0.3188	0.2353	0.8853
			Testing	0.8847	0.9354	0.3304	0.2658	0.9096
ANN2	GD	7-13-1	Training	0.9188	0.9560	0.2692	0.2085	0.7477
			Testing	0.7592	0.8548	0.4741	0.3701	1.2935
ANN3	GDA	7-11-1	Training	0.7875	0.8726	0.4203	0.3057	1.1674
			Testing	0.8045	0.8868	0.4077	0.3363	1.1369
ANN4	GDX	7-5-1	Training	0.9159	0.9544	0.2738	0.2081	0.7604
			Testing	0.7298	0.8382	0.4950	0.3860	1.3643
ANN5	RP	7-2-1	Training	0.8906	0.9379	0.3106	0.2238	0.8624
			Testing	0.8566	0.9221	0.3766	0.2913	1.0471
ANN6	SCG	7-4-1	Training	0.8023	0.8760	0.4077	0.3049	1.1324
			Testing	0.7402	0.8533	0.4808	0.3734	1.3399
WOA-ANN	**WOA**	**(20, 1500)**	**Training**	**0.9451**	**0.9709**	**0.2232**	**0.1088**	**0.6195**
			Testing	**0.9391**	**0.9683**	**0.2406**	**0.1847**	**0.6688**
LSSVR1	Polynomial kernel	–	Training	0.8403	0.9026	0.3711	0.2649	1.0307
			Testing	0.8812	0.9067	0.3522	0.3049	0.9678
LSSVR2	Linear kernel	–	Training	0.6955	0.7969	0.4902	0.3808	1.3615
			Testing	0.6987	0.7909	0.4930	0.4075	1.3728
LSSVR3	RBF kernel	–	Training	0.8390	0.9015	0.3725	0.2651	1.0345
			Testing	0.8854	0.9132	0.3416	0.2939	0.9441

Note: GD: Gradient descent
RBF: Radial Basis Function
RP: Resilient back-propagation
WOA:Whale optimization algorithm
LM: Levenberg-Marquardt
Structure: Achitecture of the ANN models

Bold item: The optimal solution

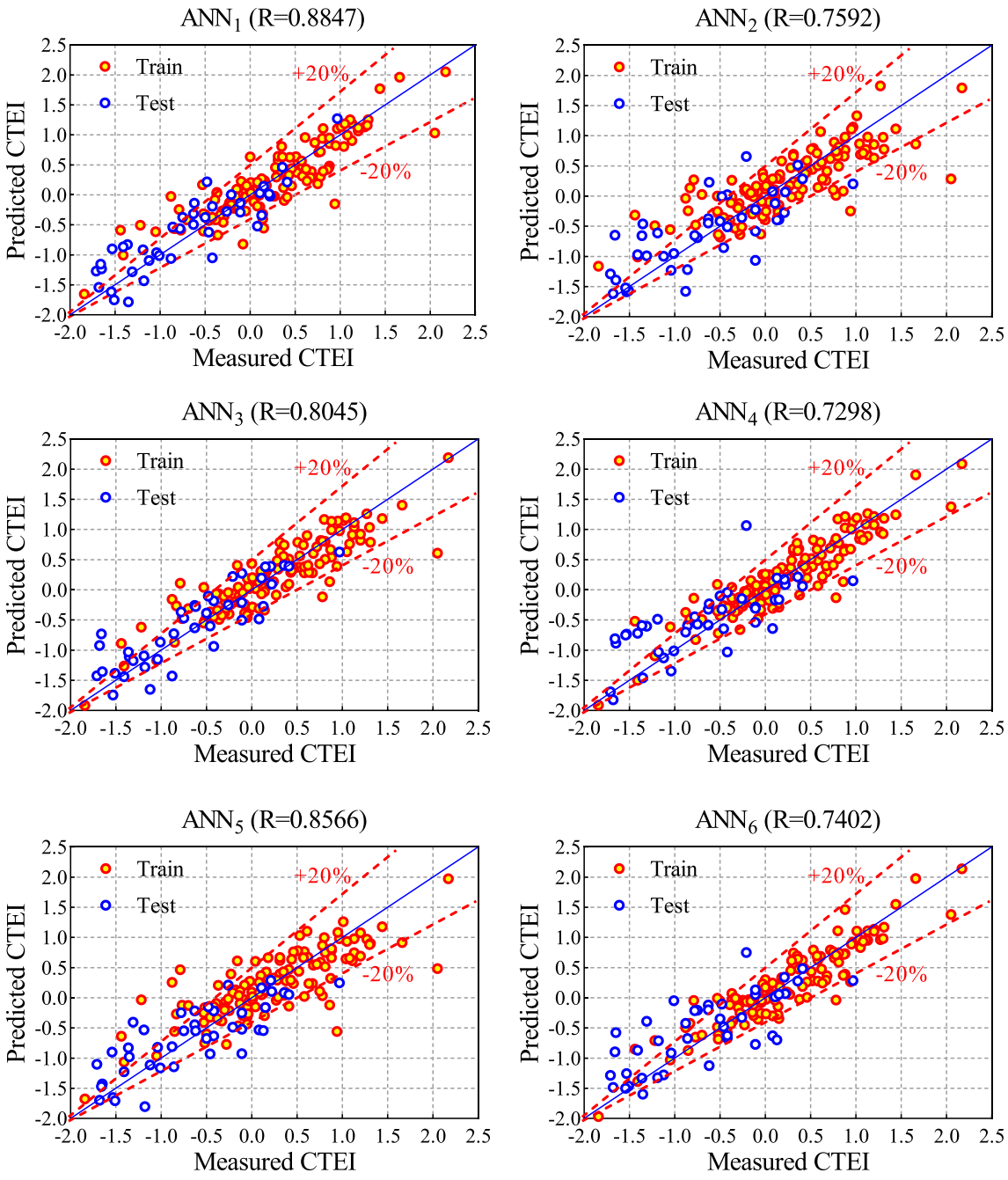

Fig.9. Scatter plots of ANN models assessment for various training function.

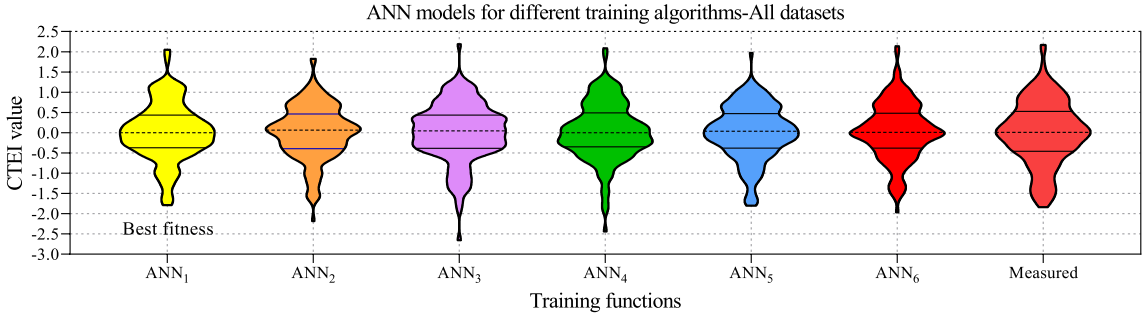

Fig. 10. The ANN performance evaluation in comparison with measured monthly CTEI.

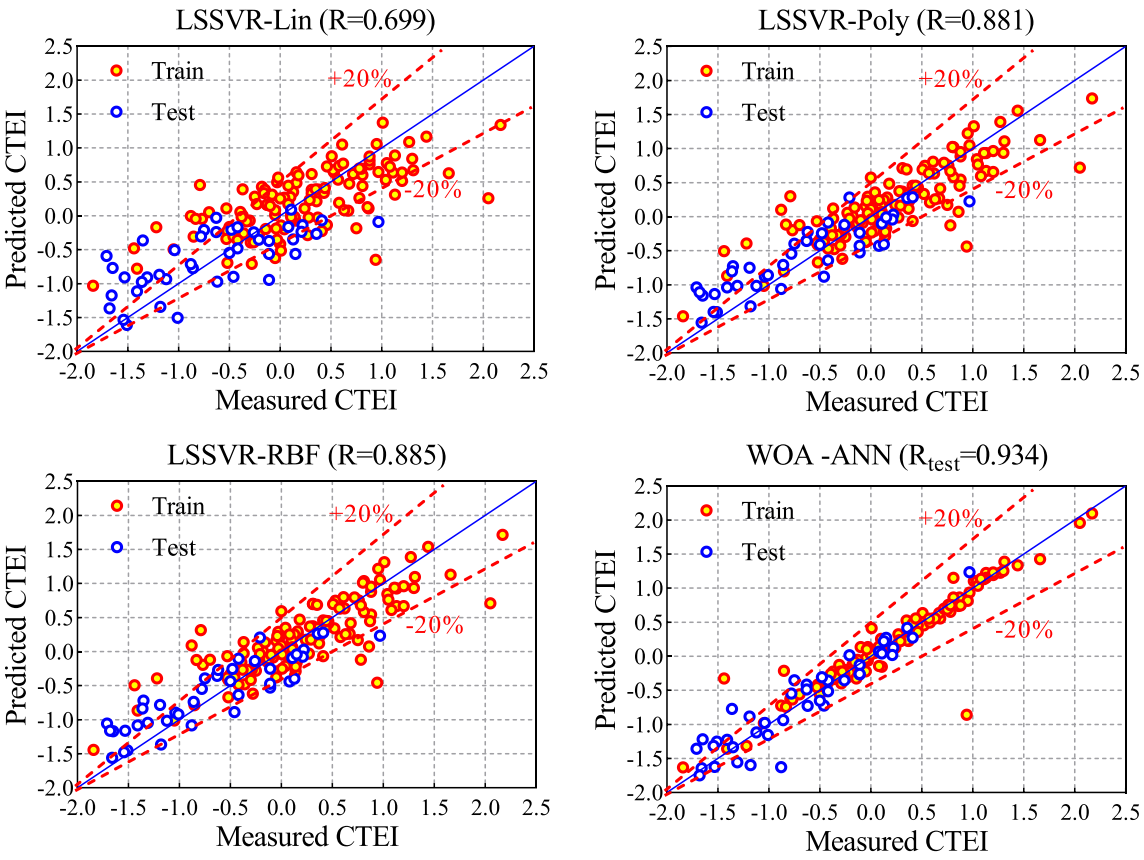

Fig. 11. The scatter plots of LSSVR and WOA-ANN models for prediction of CTEI.

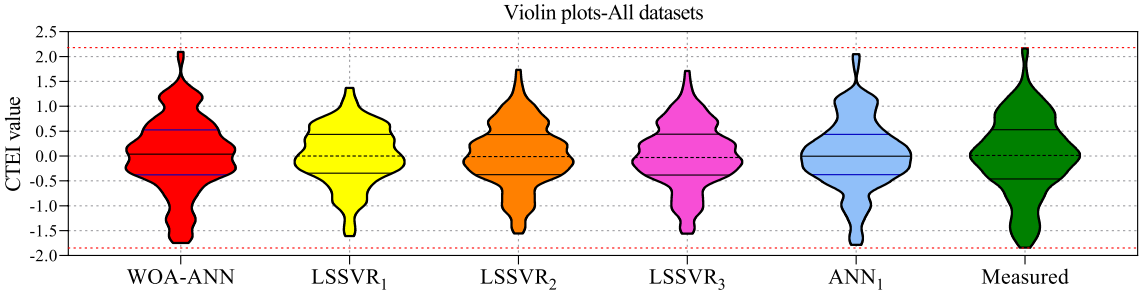

Fig. 12. The violin plots of PDF for measured and predicted monthly CTEI values.

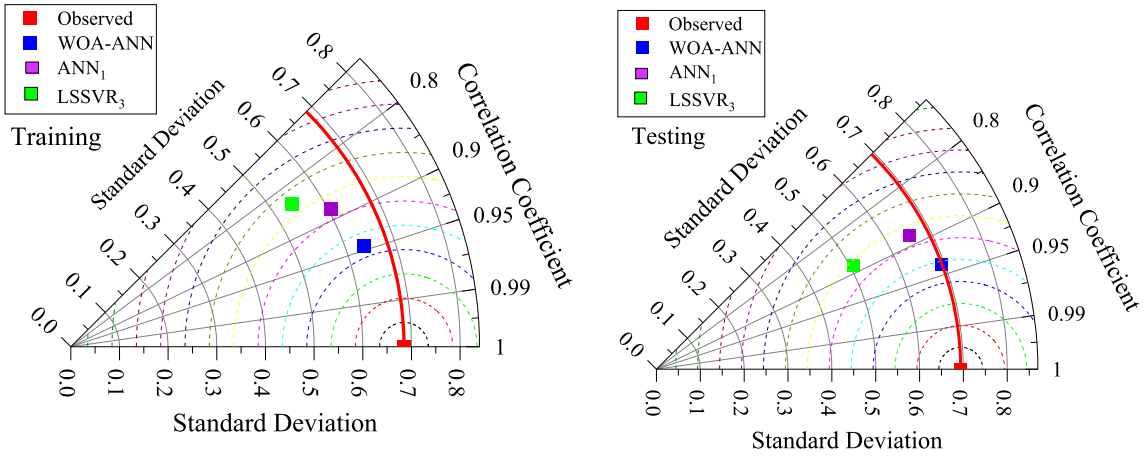

Fig. 13. Taylor diagrams of superior ML models in training (Left side) and testing (Right side) stages for prediction Of CTEI in Combo 6.

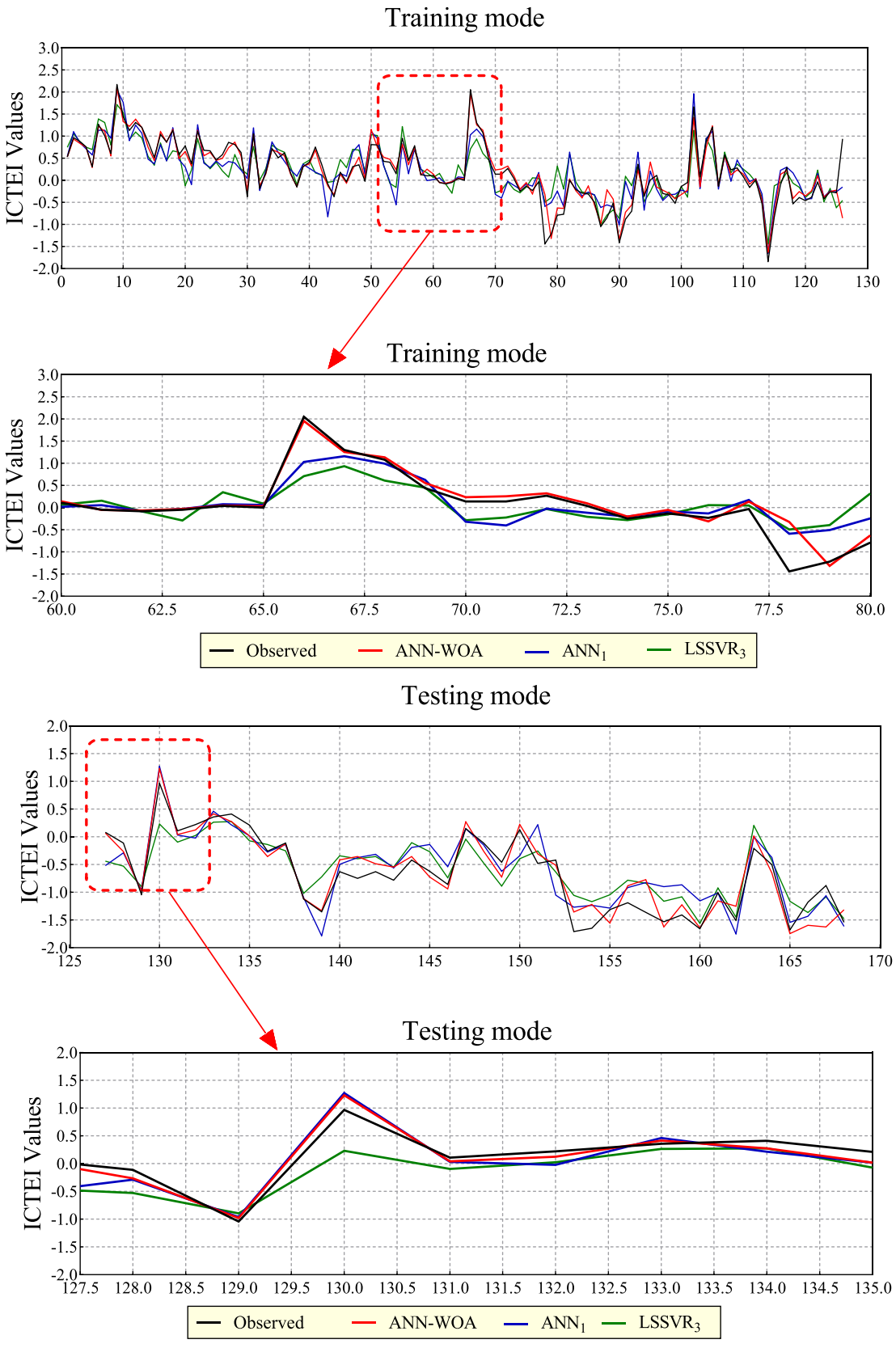

Fig. 14. The physical expect the trend of monthly CTEI in the best ANN and LSSVR models in comparison with WOA-ANN and observed values for training (Upper panel) and testing (Lower panel) phases.

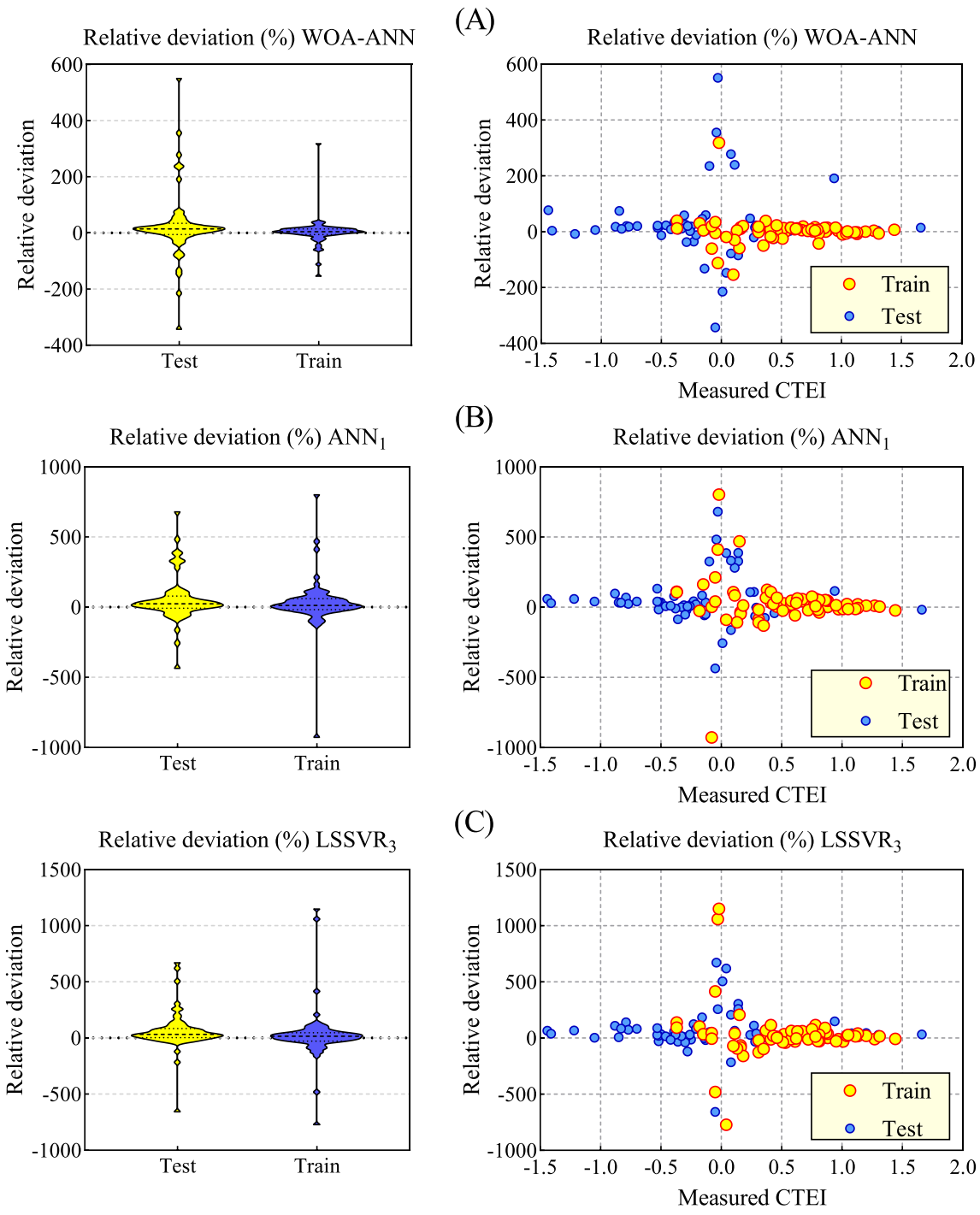

Fig. 15. The relative deviation distribution for training and testing in all selective models.

candidate inputs (modeled by the WOA-ANN) yielded the most promising accuracy, whereas, in (Elbeltagi et al., 2021), the superior outcome (SVR) was obtained based on eleven candidate inputs. It can be concluded that employing the WOA-ANN model enhanced the accuracy of CTEI simulation and reduced the candidate input parameters compared to (Elbeltagi et al., 2021).

4. Conclusion and remarks

The multiplicity of different variables in drought has complicated this phenomenon, and as a result, its prediction has become one of the significant challenges facing decision-makers. This study predicted monthly CTEI as a representative of meteorological, hydrological, and agricultural droughts by WOA-ANN, standalone ANN, and LSSVR approaches in the Ganga river basin during a period of 13 years of 2003 to 2016. At the first stage, among the total of 11 candidate input variables, including meteorological and satellite data, the number of 10 input combinations was extracted among all possible ones based on the Pearson correlation analysis and a novel FS technique, namely, relief-based algorithm. Then, the selected combinations were evaluated by a standalone ANN model (using LM training algorithm) to find the optimal combination. The outcome analysis ascertained that the ANN-based on Combo 6 (considering the GWSA, P, Air Temp, NR, SWN, LWN, PET as candidate input parameters) yielded the most promising accuracy (R =

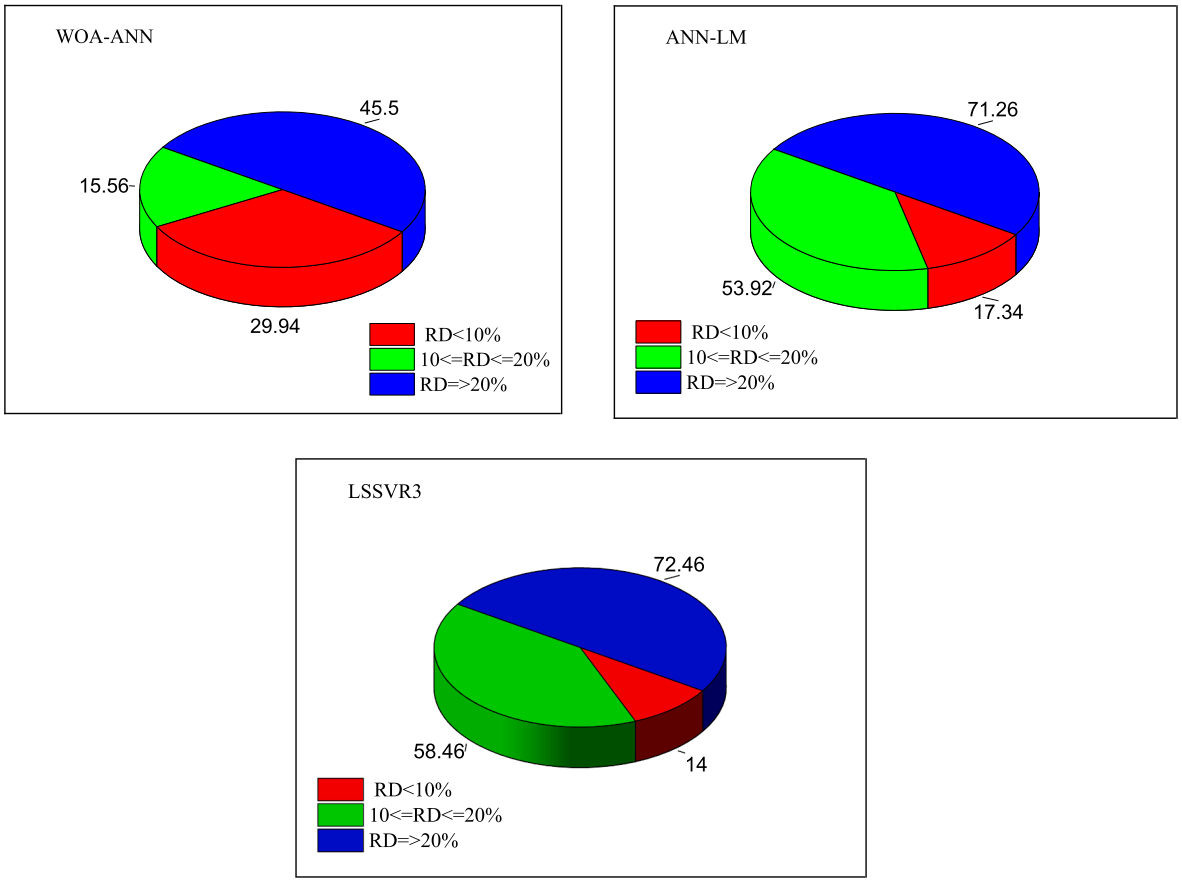

Fig. 16. CFARD for the best ML-based models for simulation of monthly CTEI.

0.8847, RMSE = 0.3304, and $U_{95\%}$ = 0.9096) among all other candidate input combinations. In the second stage of modeling, the WOA-ANN, ANN by six training algorithms (i.e., LM, SCG, RP, GDX, DDA, and GD), and LSSVR by three types of kernel function were examined to predict monthly CTEI. The different evaluation indicated that the WOA-ANN in terms of (R = 0.9391 and RMSE = 0.2406) outperformed the ANN1 (R = 0.8847 and RMSE = 0.3188) and LSSVR3 (R = 0.0.8854 and RMSE = 0.3416), respectively, for predicting CTEI. Furthermore, comparing the results of the current study with Elbetagi et al.(Elbeltagi et al., 2021) proved that WOA-ANN could achieve more precision employing fewer input parameters. The results of this study can predict future drought scenarios for managers and help reduce drought risks in the region. Future research should evaluate new architectures of the proposed hybrid model for other areas. Achieving a comprehensive model for predicting drought in areas with different climates will be critical in water resources management.

CRediT authorship contribution statement

Mehdi Jamei: Conceptualization, Software, Visualization, Writing – original draft, Writing – review & editing, Formal analysis, Supervision. **Ahmed Elbeltagi:** Conceptualization, Writing – original draft. **Saman Maroufpoor:** Software, Investigation, Writing – original draft, Writing – review & editing. **Masoud Karbasi:** Writing – review & editing. **Mozhdeh Jamei:** Writing – original draft, Writing – review & editing. **Mohammadnabi Jalali:** Writing – original draft, Writing – review & editing. **Negin Najafzadeh:** Writing – original draft, Writing – review & editing.

Declaration of Competing Interest

The authors declare that they have no known competing financial interests or personal relationships that could have appeared to influence the work reported in this paper.

References

Ahmadalipour, A., Moradkhani, H., Castelletti, A., Magliocca, N., 2019. Future drought risk in Africa: Integrating vulnerability, climate change, and population growth. Sci. Total Environ. 662, 672–686.

Ali, M., Deo, R.C., Downs, N.J., Maraseni, T., 2018. Multi-stage committee based extreme learning machine model incorporating the influence of climate parameters and seasonality on drought forecasting. Comput. Electron. Agric. 152, 149–165.

Ali, Z., Hussain, I., Faisal, M., Nazir, H.M., Hussain, T., Shad, M.Y., Mohamd Shoukry, A., Hussain Gani, S., 2017. Forecasting drought using multilayer perceptron artificial neural network model. Adv. Meteorol. 2017.

Allen, R.G., Perieira, L.S., Raes, D., Smith, M., 2006. Irrigation and Drainage Paper Crop No. 56.

Alley, W.M., 1984. The Palmer drought severity index: limitations and assumptions. J. Clim. Appl. Meteorol. 23 (7), 1100–1109.

Amjady, N., Keynia, F., 2009. Day-ahead price forecasting of electricity markets by a new feature selection algorithm and cascaded neural network technique. Energy Convers. Manag. 50 (12), 2976–2982.

Anand, J., Gosain, A.K., Khosa, R., Srinivasan, R., 2018. Regional scale hydrologic modeling for prediction of water balance, analysis of trends in streamflow and variations in streamflow: The case study of the Ganga River basin. J. Hydrol. Reg. Stud. 16, 32–53. https://doi.org/10.1016/j.ejrh.2018.02.007.

Bacanli, U.G., Firat, M., Dikbas, F., 2009. Adaptive neuro-fuzzy inference system for drought forecasting. Stoch. Environ. Res. Risk Assess. 23 (8), 1143–1154.

Beyaztas, U., Yaseen, Z.M., 2019. Drought interval simulation using functional data analysis. J. Hydrol. 579, 124141. https://doi.org/10.1016/j.jhydrol.2019.124141.

Bhanja, S.N., Mukherjee, A., Rodell, M., 2020. Groundwater storage change detection from in situ and GRACE-based estimates in major river basins across India. Hydrol. Sci. J. 65 (4), 650–659. https://doi.org/10.1080/02626667.2020.1716238.

Botai, C., Botai, J., Dlamini, L., Zwane, N., Phaduli, E., 2016. Characteristics of droughts in South Africa: a case study of free state and north west provinces. Water 8 (10), 439. https://doi.org/10.3390/w8100439.

Chen, F., Mitchell, K., Schaake, J., Xue, Y., Pan, H.-L., Koren, V., Duan, Q.Y., Ek, M., Betts, A., 1996. Modeling of land surface evaporation by four schemes and comparison with FIFE observations. J. Geophys. Res. Atmos. 101 (D3), 7251–7268. https://doi.org/10.1029/95JD02165.

Cifuentes, J., Marulanda, G., Bello, A., Reneses, J., 2020. Air temperature forecasting using machine learning techniques: a review. Energies 13 (16), 4215. https://doi.org/10.3390/en13164215.

Cortes, C., Vlagimir, V., 1995. Support-vector networks. Mach. Leaming 20 (3), 273–297.

Coulibaly, P., Anctil, F., Bobée, B., 2011. Prévision Hydrologique par Réseaux de Neurones Artificiels: État de l'Art. Can. J. Civ. Eng. 26, 293–304. https://doi.org/10.1139/cjce-26-3-293.

Cutore, P., Di Mauro, G., Cancelliere, A., 2009. Forecasting palmer index using neural networks and climatic indexes. J. Hydrol. Eng. 14 (6), 588–595.

Dai, Y., Zeng, X., Dickinson, R.E., Baker, I., Bonan, G.B., Bosilovich, M.G., Denning, A.S., Dirmeyer, P.A., Houser, P.R., Niu, G., Oleson, K.W., Schlosser, C.A., Yang, Z.-L., 2003. The common land model. Bull. Am. Meteorol. Soc. 84 (8), 1013–1024. https://doi.org/10.1175/BAMS-84-8-1013.

De Kauwe, M.G., Medlyn, B.E., Ukkola, A.M., Mu, M., Sabot, M.E.B., Pitman, A.J., Meir, P., Cernusak, L.A., Rifai, S.W., Choat, B., Tissue, D.T., Blackman, C.J., Li, X., Roderick, M., Briggs, P.R., 2020. Identifying areas at risk of drought-induced tree mortality across South-Eastern Australia. Glob. Chang. Biol. 26 (10), 5716–5733.

Deng, J., Chen, X., Du, Z., Zhang, Y., 2011. Soil water simulation and predication using stochastic models based on LS-SVM for red soil region of China. Water Resour. Manag. 25 (11), 2823–2836.

Deo, R.C., Şahin, M., 2015. Application of the extreme learning machine algorithm for the prediction of monthly Effective Drought Index in eastern Australia. Atmos. Res. 153, 512–525.

Deo, R.C., Tiwari, M.K., Adamowski, J.F., Quilty, J.M., 2017. Forecasting effective drought index using a wavelet extreme learning machine (W-ELM) model. Stoch. Environ. Res. risk Assess. 31 (5), 1211–1240.

Dharpure, J.K., Goswami, A., Patel, A., Kulkarni, A.V., Meloth, T., 2020. Drought characterization using the Combined Terrestrial Evapotranspiration Index over the Indus, Ganga and Brahmaputra river basins. Geocarto Int. 1–25.

Ek, M.B., Mitchell, K.E., Lin, Y., Rogers, E., Grunmann, P., Koren, V., Gayno, G., Tarpley, J.D., 2003. Implementation of Noah land surface model advances in the National Centers for Environmental Prediction operational mesoscale Eta model. J. Geophys. Res. 108 (D22) https://doi.org/10.1029/2002JD003296.

Elbeltagi, A., Kumari, N., Dharpure, J., Mokhtar, A., Alsafadi, K., Kumar, M., Mehdinejadiani, B., Ramezani Etedali, H., Brouziyne, Y., Towfiqul Islam, A., Kuriqi, A., 2021. Prediction of combined terrestrial evapotranspiration index (CTEI) over large river basin based on machine learning approaches. Water 13 (4), 547. https://doi.org/10.3390/w13040547.

Elbeltagi, A., Aslam, M.R., Mokhtar, A., Deb, P., Abubakar, G.A., Kushwaha, N.L., Venancio, L.P., Malik, A., Kumar, N., Deng, J., 2020. Spatial and temporal variability analysis of green and blue evapotranspiration of wheat in the Egyptian Nile Delta from 1997 to 2017. J. Hydrol. 594, 125662. https://doi.org/10.1016/j.jhydrol.2020.125662.

Fundel, F., Jörg-Hess, S., Zappa, M., 2013. Monthly hydrometeorological ensemble prediction of streamflow droughts and corresponding drought indices. Hydrol. Earth Syst. Sci. 17 (1), 395–407.

Haykin, S.S., 2009. Neural networks and learning machines/Simon Haykin.

Huffman, G.J., Bolvin, D.T., Nelkin, E.J., Wolff, D.B., Adler, R.F., Gu, G., Hong, Y., Bowman, K.P., Stocker, E.F., 2007. The TRMM Multisatellite Precipitation Analysis (TMPA): Quasi-Global, Multiyear, Combined-Sensor Precipitation Estimates at Fine Scales. J. Hydrometeorol. 8, 38–55. https://doi.org/10.1175/JHM560.1.

Ide, T., 2018. Climate war in the Middle East? Drought, the Syrian civil war and the state of climate-conflict research. Curr. Clim. Chang. reports 4 (4), 347–354.

India-WRIS, 2012. River basin atlas of India. RRSC-West, NRSC, ISRO, Jodhpur, India.

Jamei, M., Ahmadianfar, I., Karbasi, M., Jawad, A.H., Farooque, A.A., Yaseen, Z.M., 2021. The assessment of emerging data-intelligence technologies for modeling Mg+2 and SO4−2 surface water quality. J. Environ. Manage. 300, 113774. https://doi.org/10.1016/j.jenvman.2021.113774.

Jamei, M., Baygi, M.M., Oskouei, E.A., Lopez-Baeza, E., 2020. Validation of the SMOS level 1C brightness temperature and level 2 soil moisture data over the west and southwest of Iran. Remote Sens. 12, 1–20. https://doi.org/10.3390/rs12172819.

Jia, S., Zhu, W., Lű, A., Yan, T., 2011. A statistical spatial downscaling algorithm of TRMM precipitation based on NDVI and DEM in the Qaidam Basin of China. Remote Sens. Environ. 115 (12), 3069–3079. https://doi.org/10.1016/j.rse.2011.06.009.

Karbasi, M., Jamei, M., Ahmadianfar, I., Asadi, A., 2021a. Toward the accurate estimation of elliptical side orifice discharge coefficient applying two rigorous kernel-based data-intelligence paradigms. Sci. Rep. 11, 1–18.

Karbasi, M., Karbasi, M., Jamei, M., Malik, A., Azamathulla, H.M., 2021b. Development of a new wavelet-based hybrid model to forecast multi-scalar SPEI drought index (case study: Zanjan city, Iran). Theor. Appl. Climatol. 1–24.

Keskin, M.E., Terzi, O., Taylan, E.D., Küçükyaman, D., 2009. Meteorological drought analysis using data-driven models for the Lakes District, Turkey. Hydrol. Sci. J. 54 (6), 1114–1124.

Khan, A., Koch, M., Chinchilla, K., 2018. Evaluation of Gridded Multi-Satellite Precipitation Estimation (TRMM-3B42-V7) Performance in the Upper Indus Basin (UIB). Climate 6, 76. https://doi.org/10.3390/cli6030076.

Khan, N., Sachindra, D.A., Shahid, S., Ahmed, K., Shiru, M.S., Nawaz, N., 2020. Prediction of droughts over Pakistan using machine learning algorithms. Adv. Water Resour. 139, 103562. https://doi.org/10.1016/j.advwatres.2020.103562.

Kira, K., Rendell, L.A., 1992. A practical approach to feature selection. In: Machine Learning Proceedings 1992. Elsevier, pp. 249–256. https://doi.org/10.1016/B978-1-55860-247-2.50037-1.

Kisi, O., Docheshmeh Gorgij, A., Zounemat-Kermani, M., Mahdavi-Meymand, A., Kim, S., 2019. Drought forecasting using novel heuristic methods in a semi-arid environment. J. Hydrol. 578, 124053. https://doi.org/10.1016/j.jhydrol.2019.124053.

Kononenko, I., 1994. Estimating attributes: Analysis and extensions of RELIEF. In: European Conference on Machine Learning. Springer, pp. 171–182.

Koster, R.D., Suarez, M.J., 1996. Energy and Water Balance Calculations in the Mosaic LSM. NASA Tech. Memo. 9, 76.

Kousari, M.R., Hosseini, M.E., Ahani, H., Hakimelahi, H., 2017. Introducing an operational method to forecast long-term regional drought based on the application of artificial intelligence capabilities. Theor. Appl. Climatol. 127 (1-2), 361–380.

Leblanc, M.J., Tregoning, P., Ramillien, G., Tweed, S.O., Fakes, A., 2009. Basin-scale, integrated observations of the early 21st century multiyear drought in Southeast Australia. Water Resour. Res. 45, 1–10. https://doi.org/10.1029/2008WR007333.

Li, Z., Chen, T., Wu, Q.i., Xia, G., Chi, D., 2020. Application of penalized linear regression and ensemble methods for drought forecasting in Northeast China. Meteorol. Atmos. Phys. 132 (1), 113–130. https://doi.org/10.1007/s00703-019-00675-8.

Liu, Y.i., Zhu, Y.e., Ren, L., Yong, B., Singh, V.P., Yuan, F., Jiang, S., Yang, X., 2019. On the mechanisms of two composite methods for construction of multivariate drought indices. Sci. Total Environ. 647, 981–991.

Long, D., Yang, Y., Wada, Y., Hong, Y., Liang, W., Chen, Y., Yong, B., Hou, A., Wei, J., Chen, L., 2015. Deriving scaling factors using a global hydrological model to restore GRACE total water storage changes for China's Yangtze River Basin. Remote Sens. Environ. 168, 177–193. https://doi.org/10.1016/j.rse.2015.07.003.

Madadgar, S., Moradkhani, H., 2014. Spatio-temporal drought forecasting within Bayesian networks. J. Hydrol. 512, 134–146.

Malik, A., Kumar, A., 2020. Meteorological drought prediction using heuristic approaches based on effective drought index: a case study in Uttarakhand. Arab. J. Geosci. 13, 1–17. https://doi.org/10.1007/s12517-020-5239-6.

Malik, A., Kumar, A., Rai, P., Kuriqi, A., 2021a. Prediction of Multi-Scalar Standardized Precipitation Index by Using Artificial Intelligence and Regression Models. Climate 9 (2), 28. https://doi.org/10.3390/cli9020028.

Malik, A., Kumar, A., Salih, S.Q., Kim, S., Kim, N.W., Yaseen, Z.M., Singh, V.P., 2020. Drought index prediction using advanced fuzzy logic model: Regional case study over Kumaon in India. PLoS One 15, e0233280. https://doi.org/10.1371/journal.pone.0233280.

Malik, A., Tikhamarine, Y., Al-Ansari, N., Shahid, S., Sekhon, H.S., Pal, R.K., Rai, P., Pandey, K., Singh, P., Elbeltagi, A., Sammen, S.S., 2021b. Daily pan-evaporation estimation in different agro-climatic zones using novel hybrid support vector regression optimized by Salp swarm algorithm in conjunction with gamma test. Eng. Appl. Comput. Fluid Mech. 15 (1), 1075–1094. https://doi.org/10.1080/19942060.2021.1942990.

Malik, A., Tikhamarine, Y., Sammen, S.S., Abba, S.I., Shahid, S., 2021c. Prediction of meteorological drought by using hybrid support vector regression optimized with HHO versus PSO algorithms. Environ. Sci. Pollut. Res. 28 (29), 39139–39158.

Malik, A., Tikhamarine, Y., Souag-Gamane, D., Rai, P., Sammen, S.S., Kisi, O., 2021d. Support vector regression integrated with novel meta-heuristic algorithms for meteorological drought prediction. Meteorol. Atmos. Phys. 133 (3), 891–909.

Malik, H., Yadav, A.K., 2021. A novel hybrid approach based on relief algorithm and fuzzy reinforcement learning approach for predicting wind speed. Sustain. Energy Technol. Assessments 43, 100920. https://doi.org/10.1016/j.seta.2020.100920.

McKee, T.B., Doesken, N.J., Kleist, J., 1993. The relationship of drought frequency and duration to time scales, in: Proceedings of the 8th Conference on Applied Climatology. Boston, pp. 179–183.

Maroufpoor, S, Sanikhani, H., Kisi, O., C Deo, R. and Zaher Mundher, Y., 2019. Long-term modelling of wind speeds using six different heuristic artificial intelligence approaches. International Journal of Climatology 39 (8), 3543–3557. https://doi.org/10.1002/joc.6037.

Mirjalili, S., Lewis, A., 2016. The Whale Optimization Algorithm. Adv. Eng. Softw. 95, 51–67. https://doi.org/10.1016/j.advengsoft.2016.01.008.

Mirjalili, S., Mohd Hashim, S.Z., Moradian Sardroudi, H., 2012. Training feedforward neural networks using hybrid particle swarm optimization and gravitational search algorithm. Appl. Math. Comput. 218 (22), 11125–11137. https://doi.org/10.1016/j.amc.2012.04.069.

Mishra, A.K., Desai, V.R., Singh, V.P., 2007. Drought forecasting using a hybrid stochastic and neural network model. J. Hydrol. Eng. 12 (6), 626–638.

Mishra, A.K., Singh, V.P., 2011. Drought modeling–A review. J. Hydrol. 403 (1-2), 157–175.

Miyan, M.A., 2015. Droughts in Asian least developed countries: Vulnerability and sustainability. Weather Clim. Extrem. 7, 8–23.

Mohamed, Ahmed, Karem, Abdelmohsen, 2018. Quantifying Modern Recharge and Depletion Rates of the Nubian Aquifer in Egypt. Surveys in Geophysics 39, 729–751. https://doi.org/10.1007/s10712-018-9465-3.

Mokhtarzad, M., Eskandari, F., Vanjani, N.J., Arabasadi, A., 2017. Drought forecasting by ANN, ANFIS, and SVM and comparison of the models. Environ. earth Sci. 76, 729.

Morid, S., Smakhtin, V., Bagherzadeh, K., 2007. Drought forecasting using artificial neural networks and time series of drought indices. Int. J. Climatol. A J. R. Meteorol. Soc. 27, 2103–2111.

Mulualem, G.M., Liou, Y.-A., 2020. Application of Artificial Neural Networks in Forecasting a Standardized Precipitation Evapotranspiration Index for the Upper Blue Nile Basin. Water 12, 643.

Muñoz-Sabater, J., Dutra, E., Agustí-Panareda, A., Albergel, C., Arduini, G., Balsamo, G., Boussetta, S., Choulga, M., Harrigan, S., Hersbach, H., Martens, B., Miralles, D., Piles, M., Rodríguez-Fernández, N., Zsoter, E., Buontempo, C., Thépaut, J.-N., 2021. ERA5-Land: A state-of-the-art global reanalysis dataset for land applications. Earth Syst. Sci. Data Discuss. 1–50 https://doi.org/10.5194/essd-2021-82.

Naseri, A., Jamei, M., … I.A.-E. with, 2020, U., n.d. Nanofluids thermal conductivity prediction applying a novel hybrid data-driven model validated using Monte Carlo-based sensitivity analysis. Springer.
Nguyen, V., Li, Q., Nguyen, L., 2017. Drought forecasting using ANFIS-a case study in drought prone area of Vietnam. Paddy Water Environ. 15, 605–616.
Özger, M., Başakın, E.E., Ekmekcioğlu, Ö., Hacısüleyman, V., 2020. Comparison of wavelet and empirical mode decomposition hybrid models in drought prediction. Comput. Electron. Agric. 179, 105851.
Özger, M., Mishra, A.K., Singh, V.P., 2012. Long lead time drought forecasting using a wavelet and fuzzy logic combination model: a case study in Texas. J. Hydrometeorol. 13, 284–297.
Papacharalampous, G., Tyralis, H., Koutsoyiannis, D., 2018. Univariate time series forecasting of temperature and precipitation with a focus on machine learning algorithms: A multiple-case study from Greece. Water Resour. Manag. 32, 5207–5239.
Robnik-Šikonja, M., Kononenko, I., 2003. Theoretical and empirical analysis of ReliefF and RReliefF. Mach. Learn. 53, 23–69.
Rodell, M., Chen, J., Kato, H., Famiglietti, J.S., Nigro, J., Wilson, C.R., 2007. Estimating groundwater storage changes in the Mississippi River basin (USA) using GRACE. Hydrogeol. J. 15, 159–166. https://doi.org/10.1007/s10040-006-0103-7.
Rodell, M., Houser, P.R., Jambor, U., Gottschalck, J., Mitchell, K., Meng, C.J., Arsenault, K., Cosgrove, B., Radakovich, J., Bosilovich, M., Entin, J.K., Walker, J.P., Lohmann, D., Toll, D., 2004. The Global Land Data Assimilation System. Am. Meteorol. Soc.
Rui, H.L., Beaudoing, H., 2020. README Document for NASA GLDAS Version 2 Data Products. Goddard Earth Sci. Data Inf. Serv. Cent. (GES DISC) 16, 1–32.
Shrestha, A.B., Agrawal, N.K., Alfthan, B., Bajracharya, S.R., Maréchal, J., van Oort, B., 2015. The Himalayan Climate and Water Atlas.
Shuttlewor, W.J., 1992. Evaporation, McGRAW-HILL, Handbook of Hydrology. https://doi.org/10.1007/978-3-642-41714-6_80111.
Sinha, D., Syed, T.H., Reager, J.T., 2019. Utilizing combined deviations of precipitation and GRACE-based terrestrial water storage as a metric for drought characterization: A case study over major Indian river basins. J. Hydrol. 572, 294–307. https://doi.org/10.1016/J.JHYDROL.2019.02.053.
Sun, A.Y., Scanlon, B.R., Zhang, Z., Walling, D., Bhanja, S.N., Mukherjee, A., Zhong, Z., 2019. Combining Physically Based Modeling and Deep Learning for Fusing GRACE Satellite Data: Can We Learn From Mismatch? Water Resour. Res. 1179–1195. https://doi.org/10.1029/2018WR023333.
Suykens, K., Vandewalle, J., 2000. Least Squares Support Vector Machine Classifiers. Ann. Oper. Res. 97, 131–141. https://doi.org/10.1023/A.
Thomas, A.C., Reager, J.T., Famiglietti, J.S., Rodell, M., n.d. A GRACE-based water storage deficit approach for hydrological drought characterization. https://doi.org/10.1002/2014GL059323.
Tiwari, V.M., Wahr, J., Swenson, S., 2009. Dwindling groundwater resources in northern India, from satellite gravity observations. Geophys. Res. Lett. 36, 1–5. https://doi.org/10.1029/2009GL039401.
Trambauer, P., Maskey, S., Winsemius, H., Werner, M., Uhlenbrook, S., 2013. A review of continental scale hydrological models and their suitability for drought forecasting in (sub-Saharan) Africa. Phys. Chem. Earth, Parts A/B/C 66, 16–26.
Tsakiris, G., Vangelis, H., 2005. Establishing a drought index incorporating evapotranspiration. Eur. water 9, 3–11.
Vicente-Serrano, S.M., Beguería, S., López-Moreno, J.I., 2010. A multiscalar drought index sensitive to global warming: the standardized precipitation evapotranspiration index. J. Clim. 23, 1696–1718.
Vidyarthi, V.K., Jain, A., Chourasiya, S., n.d. Modeling rainfall-runoff process using artificial neural network with emphasis on parameter sensitivity.
Wilhite, D.A., Glantz, M.H., 1985. Understanding: the drought phenomenon: the role of definitions. Water Int. 10, 111–120.
Xu, Liang, Zhenghui, Xie, Maoyi, Huang, 2003. A new parameterization for surface and groundwater interactions and its impact on water budgets with the variable infiltration capacity (VIC) land surface model. Journal of Geophysical Research: Atmospheres 108 (D16).
Yang, P., Xia, J., Zhan, C., Qiao, Y., Wang, Y., 2017. Monitoring the spatio-temporal changes of terrestrial water storage using GRACE data in the Tarim River basin between 2002 and 2015. Sci. Total Environ. 595, 218–228. https://doi.org/10.1016/j.scitotenv.2017.03.268.
Yaseen, Z.M., Ali, M., Sharafati, A., Al-Ansari, N., Shahid, S., 2021. Forecasting standardized precipitation index using data intelligence models: regional investigation of Bangladesh. Sci. Rep. 11, 1–25.
Yaseen, Z.M., Allawi, M.F., Yousif, A.A., Jaafar, O., Hamzah, F.M., El-Shafie, A., 2018. Non-tuned machine learning approach for hydrological time series forecasting. Neural Comput. Appl. 30, 1479–1491.
Yaseen, Z.M., Shahid, S., 2020. Drought Index Prediction Using Data Intelligent Analytic Models: A Review. Springer Trans. Civ. Environ. Eng. https://doi.org/10.1007/978-981-15-5772-9_1.
Zengir, V.S., Sobhani, B., Asghari, S., 2020. Monitoring and investigating the possibility of forecasting drought in the western part of Iran. Arab. J. Geosci. 13, 1–12.
Zhang, B., Long, B., Wu, Z., Wang, Z., 2017. An evaluation of the performance and the contribution of different modified water demand estimates in drought modeling over water-stressed regions. L. Degrad. Dev. 28, 1134–1151.
Zhang, J.R., Zhang, J., Lok, T.M., Lyu, M.R., 2007. A hybrid particle swarm optimization-back-propagation algorithm for feedforward neural network training. Appl. Math. Comput. 185, 1026–1037. https://doi.org/10.1016/j.amc.2006.07.025.
Zhang, R., Chen, Z.-Y., Xu, L.-J., Ou, C.-Q., 2019a. Meteorological drought forecasting based on a statistical model with machine learning techniques in Shaanxi province, China. Sci. Total Environ. 665, 338–346.
Zhang, Y., Yang, H., Cui, H., Chen, Q., 2019b. Comparison of the Ability of ARIMA, WNN and SVM Models for Drought Forecasting in the Sanjiang Plain, China. Nat. Resour. Res. 29, 1447–1464. https://doi.org/10.1007/s11053-019-09512-6.
Zhao, C., Brissette, F., Chen, J., Martel, J.-L., 2020. Frequency change of future extreme summer meteorological and hydrological droughts over North America. J. Hydrol. 584, 124316.